Physics – Uspekhi **64** (6) 584 – 616 (2021) ©2021 Uspekhi Fizicheskikh Nauk, Russian Academy of Sciences

REVIEWS OF TOPICAL PROBLEMS

PACS numbers: **05.45. – a**, 05.45.Tp, 05.45.Xt, 64.60.aq, 87.85.dd, 87.85.dm

Functional networks of the brain: from connectivity restoration to dynamic integration

A E Hramov, N S Frolov, V A Maksimenko, S A Kurkin, V B Kazantsev, A N Pisarchik

DOI: https://doi.org/10.3367/UFNe.2020.06.038807

Contents

1. Introduction **584**

2. Reconstruction of functional connections from experimental data on brain activity **586**

2.1 Problems and limitations inherent in the reconstruction of functional networks; 2.2 Reconstruction of brain sources to assess connections; 2.3 Hierarchy and classification of the methods for reconstructing functional connections; 2.4 Methods for assessing effective connections

3. Integration processes in the brain **597**

3.1 Mathematical apparatus of the theory of complex networks; 3.2 Functional networks formed during processing of visual sensory information; 3.3 Integration and segregation of the functional brain network in planning motor activity; 3.4 Functional interaction between brain regions before and during an epileptic seizure

4. Network brain–computer interfaces **610**

5. Conclusion **612**

References **613**

Abstract. A review of physical and mathematical methods for reconstructing the functional networks of the brain based on recorded brain activity is presented. Various methods are considered, as are their advantages and disadvantages and limitations of the application. Problems applying the theory of complex networks to reconstructed functional networks of the brain to explain the effects of dynamic integration in the brain and their influence on the diverse functionality of the brain and consciousness, as well as processes leading to the pathological activity of the central nervous system, are examined. Questions concerning the application of these approaches are considered both to describe the functioning of the brain in various cognitive and pathological processes and to create new brain–computer interfaces based on the detection of changes in functional connections in the brain.

Keywords: functional connectivity, synchronization, complex networks, neural networks, analysis of electroencephalograms and magnetoencephalograms

A E Hramov [1, 2, *], **N S Frolov** [1], **V A Maksimenko** [1], **S A Kurkin** [1], **V B Kazantsev** [1], **A N Pisarchik** [1, 3]

[1] Innopolis University,
Center for Technologies in Robotics and Mechatronics Components, Laboratory of Neuroscience and Cognitive Technologies,
ul. Universitetskaya 1, 420500 Innopolis, Tatarstan, Russian Federation

[2] V M Razumovsky Saratov State Medical University,
ul. Bolshaya Kazachia 112, 410012 Saratov, Russian Federation

[3] Center for Biomedical Technology, Universidad Politécnica de Madrid, Campus Montegancedo, Pozuelo de Alarcón, 28223 Madrid, Spain

E-mail: [*] a.hramov@innopolis.ru

Received 29 March 2020, revised 28 June 2020
Uspekhi Fizicheskikh Nauk **191** (6) 614 – 650 (2021)
Translated by Yu V Morozov

1. Introduction

The brain is a complex network in which observations on a large scale reveal several hundred regions and many thousands of interconnected pathways formed from white matter axons [1]. Studies of brain networks are motivated by the belief that brain functions are not exclusively associated with individual regions and connections, but rather arise from the topology of the network as a whole, the so-called brain connectome [2]. Despite remarkable achievements in modern molecular neurobiology and genetics, both the mechanisms and principles of brain work at the cellular-network, systemic, and functional levels in actual fact remain unclear.

Modern universally recognized physical and mathematical concepts proposed to describe brain functioning lay emphasis on the mechanisms of electrogenesis, i.e., the generation of electrical impulses (action potentials or spikes), the basic anatomical architectonics of brain structures (hippocampus, cerebellum, thalamus, cortical layers, etc.), the processes of signal propagation along nerve fibers, and the basic mechanisms of synaptic neurotransmission and plasticity [3]. They are comparatively easy to describe based on the systems of differential equations and stochastic models. However, it remains to be elucidated how these processes form brain functional systems, including both relatively simple functions, such as motor control or sensorimotor transformations, and higher cognitive functions, e.g., learning, memory, and consciousness. On the other hand, the actually measured parameters (signals of electro- and magnetoencephalography (EEG/MEG) or functional magnetic resonance imaging (fMRI)) are often rather difficult to square with cellular-network models of neuronal interactions.

One example of such a tie-in is the concept of brain rhythmic activity at the cellular level up to the functional one. It turns out that brain rhythms [4–6] determine the

possibility of implementing cognitive functions, such as associative perception, focusing of attention, and phase precession in the hippocampus for the solution of spatial navigation tasks. The list of models proposed by Russian biophysicists includes but is not limited to those of oscillatory neural networks [6], complex pulse-propagation networks with plastic connections [7, 8], nonlinear effects of synchronization, competition, chaos [9, 10], polychronization [11], and the physical and chemical foundations of cognitive functions [12]. These models describe the relationships between the cellular network organization of the brain and the dynamic processes contributing to the realization of cognitive functions. However, these are conceptual models that can not fully explain the data obtained by brain researchers using the available neuroimaging methods.

In an attempt to account for the rich brain functionality associated with a relatively stable structure of the connectome, neuroscientists are showing increasing interest in the topology of brain functional connectivity dynamically formed and rearranged between different cerebral regions during the performance of various cognitive tasks [13, 14], manipulation of working memory content [15], processing of sensory information [16], and even at rest [17]. Functional connectivity reconstructed from recorded time series of brain activity describes the statistical dependence between the dynamic patterns of individual brain regions. Time series data can be obtained by various neuroimaging methods, such as monitoring the hemodynamic response of the brain using fMRI [18] and functional near-infrared spectroscopy (fNIRS) [19], as well as by analyzing the brain's electrical or magnetic activities based on EEG [20] and MEG [21, 22] data, respectively. The functional relationships can be determined in several ways, including cross-correlation, mutual information, spectral coherence, or machine learning methods.

This review is focused on considering the most effective and widely used methods for elucidating functional connectivity (see Section 2.3 for details). To recall, although a statistical relationship between two areas of the brain is often perceived as a sign of a functional relationship, this does not necessarily imply a causal relationship [23]. The functional connectivity is nonstationary and often changes within tens or hundreds of milliseconds, since it is continuously modulated by various factors and processes in the brain, such as fatigue [24, 25], sensory stimuli [26], or cognitive task content [27]. Even when measured by methods that operate at a low sampling frequency, e.g., fMRI or fNIRS, the functional connectivity can exhibit nonstationary dynamics, e.g., in the resting state [28].

Another type of connection identified in studies on large-scale brain networks are 'effective' connections used in the reconstruction of a network of directed interactions in the brain, taking account of causality relationships between neuronal elements. Indeed, an effective brain network is an empirical mathematical model that takes into consideration the observed data and is selected from a number of possible models using objective criteria to prove the correctness of the model. Recent developments in this area resulted in the creation of approaches to 'network detection,' including the identification of mathematical graph-based models of effective brain connectivity that best explain the empirical data [29, 30].

It should be noted that the assessment of effective connections opens up great prospects for a higher-quality in-depth analysis of integrative brain dynamics; however, most modern research activities are still focused on the reconstruction and analysis of functional connectivity in the brain. Therefore, this more standard approach is the central topic of the present review.

To analyze the emerging and dynamically changing functional networks of the brain, the apparatus of the theory of complex networks based on the mathematical graph theory is widely employed. It has proven itself well in investigations of complex network structures in nonlinear physics, genetics, energy, biophysics, sociology, etc. [31, 32]. In neuroscience, such networks or graphs described as a set of nodes (brain areas) and edges (functional connections reflecting statistical relationships between them) can be analyzed using various quantitative tools and methods developed in the framework of the modern network theory [2, 33–38].

The reconstruction of functional connections between brain areas is an important step toward a concise meaningful description of brain networks and their integration in the process of cognitive activity or as a consequence of pathologies known to affect the central nervous system with the use of data obtained by various neuroimaging techniques [39–45]. Such functional networks, as well as their dynamic patterns, turn out to be very informative for solving applied problems, including medical applications (monitoring brain activity, identifying pathological and stressful conditions, diagnostics of neurodegenerative disorders, etc.), cognitive neuroscience (studying sensory information processing mechanisms, decision-making processes, planning motor activity, short-term memory operations), and neurotechnologies, including the design and creation of brain–computer interfaces [46–50]. The use of the network approach in brain research organically and naturally integrates some areas of neuroanatomy ('structural' connections in the brain [1]) and brain dynamics ('functional' and/or 'effective' connections [51]) by finding correlations between the dynamics of the brain's neuronal ensemble measured with the use of various neuroimaging methods or found mathematically (e.g., by reconnecting) and the underlying anatomical and cellular substrate.

It should be noted that the principles of information processing in the brain and the clarification and extension of relevant cellular models are quite actively discussed with reference to various fundamental and applied aspects. One of these aspects is the role of the extracellular substance in the transport of information. Ongoing experimental studies show that glial cells, such as astrocytes, are able to modulate synaptic transmission in the brain and influence information transfer processes [52]. Moreover, the extracellular matrix of the brain that serves as a framework for signal neuronal networks is also capable of modulating information transmission in cerebral structures [53]. In fact, glia and the matrix represent an active extracellular environment into which the neuronal network is submerged. The question of whether the glia and the matrix provide the necessary substrate for the generation of cognitive functions in the brain (similar to an active substance in laser generation in physics) still remains open.

An important fundamental aspect of the principles of brain work is the brain's structural plasticity. In Hebb's classical interpretation, plasticity means the ability of a neural network to enhance one pathway or another to transmit a neuronal signal, if there is a functional need for this, or to weaken it, if this pathway is not used. This concept envisages, apart from that, structural changes: whenever necessary, not only new receptors but also new synapses can be formed, which is likely to cause both correction of

connection weights and alteration of the entire network architecture. Moreover, it is believed that new elements (neurons) can be brought in from the respective stem cell storage (e.g., the dentate fascia of the hippocampus). From the standpoint of physical and mathematical descriptions, such networks must be modeled by multidimensional dynamic systems with variable dimensions, although a generally accepted technique for the purpose is yet unavailable. Nevertheless, the modern literature tends to develop, in the context of structural plasticity, models of growing neural networks that can be endowed with functional activity in the future [54, 55].

The view that the brain is a totality of complex neuron-glia networks with variable dynamic characteristics from the point of view of its macrodescription for practical (including medical) applications accentuates the problem of elucidating the dynamics of functional connections between different local brain regions performing various cognitive tasks under normal and pathological conditions. Obviously, the functional networks (described by graphs) obtained as a result of such reconstructions represent an image, albeit a rather crude one, of the activity of the corresponding neuronal-glial networks. This image, however, is a complex dynamic subject, the study of which is a nontrivial task, especially with respect to the realization of higher nervous functions for which the brain activates large neuronal ensembles. Their complexity increases exponentially with the growth of the number of neurons. As a consequence, the performance of cognitive tasks requires effective communication and integration of neural networks between distributed brain areas. Integration processes in the large-scale network of the brain develop depending on the anatomical features of neural connections, but are not limited to them.

The construction and subsequent analysis of a cerebral functional and/or effective network using the approaches of the theory of complex networks are illustrated in Fig. 1. The functional data on the dynamics of various brain regions recorded when monitoring electrical activity (the top of Fig. 1) or hemodynamic response (the bottom of Fig. 1) can be converted into a network form [56, 57]. In the case of neuroimaging with the use of fMRI, the network nodes are usually obtained by dividing the areas of cortical and subcortical gray matter with due regard for their anatomical boundaries or by specifying uniformly distributed volume elements (voxels) of a fixed size. When analyzing the brain's electrical activity based on the results of EEG/MEG or blood flow measurements in the cortical regions using fNIRS, the nodes are usually chosen naturally as the locations of sensors on the surface of the head [58]. However, this approach, called sensor level analysis, does not take into account the fact that each EEG or MEG sensor can reflect the activity of several sources of neuronal activity in the brain, representing their superposition (see Section 2.1). An alternative approach is to reconstruct the sources of neural activity from EEG/MEG data. It consists of specifying node sources by dividing the volume or the surface of the brain into areas, obtaining the corresponding time series of their dynamics, and analyzing connections at the level of reconstructed sources (see Section 2.2).

After the nodes are specified, it is possible to determine their dynamics in time characterized by time series (e.g., by changes of the potential or the magnetic field in the case of EEG or MEG, blood-oxygen-level-dependent (BOLD) signals in case of fMRI). To recall, the use of EEG/MEG is often preceded by the preliminary processing of time series, in particular, to select the frequency range of interest either by filtering or based on the wavelet transform [59, 60]. Then, the time series are used to evaluate functional or effective connections, the full set of which between all nodes can be aggregated into an adjacency matrix, which is a mathematical representation of the network graph (see Section 3.1.1). Various mathematical approaches are used to estimate the significance of connections as well as effects of segregation and integration in the brain's functional networks (see Section 3.1.2). Review articles [57, 61, 62] can be recommended for the interested reader. Section 3.1.3 discusses the formalism and principles of constructing multilayer functional brain networks. To remove insignificant or weak interactions, various methods of statistical analysis are used, specifically, the correction of statistical significance levels taking into account multiple comparisons by the permutation method [63]. Section 2 is devoted to the analysis of the main problems and approaches to the reconstruction of functional connections based on neuroimaging data.

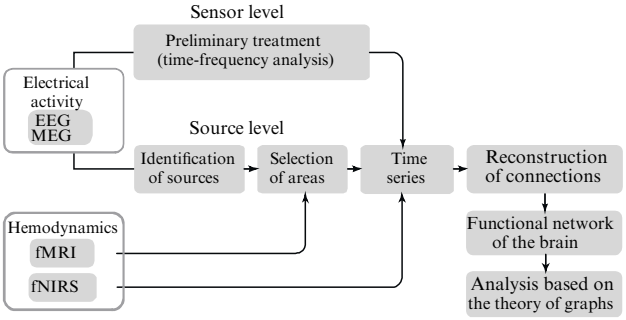

Figure 1. General scheme for constructing and analyzing the functional network of the brain using data obtained by various neuroimaging methods and approaches to examining neural processes at the level of sensors or at the level of sources of neural activity.

It can be concluded that modern network approaches, actively developed in nonlinear physics and mathematics, have enriched our understanding of brain functioning. Consideration of the application of the methods for the reconstruction and analysis of complex networks from large sets of experimental neurophysiological data is the central topic of this review. Concrete examples of investigations into emerging functional brain networks are presented in Sections 3.2–3.4; their application to the creation of multimodal and network brain–computer interfaces is briefly discussed in Section 4.

2. Reconstruction of functional connections from experimental data on brain activity

2.1 Problems and limitations inherent in the reconstruction of functional networks

A description of physical and mathematical methods for the reconstruction of functional connections should be preceded by considering problems that can significantly affect the results obtained and their interpretation. First and foremost, this concerns signals of the brain's electrical activity (MEG/EEG) and signals of local field potentials intrinsic in the nature of these signals. The limitations described below should be considered when choosing concrete methods and developing new approaches for the reconstruction of brain connections and functional networks.

2.1.1 Bulk conductivity and field propagation. This problem pertaining to the analysis of functional connections at the sensor level based on multichannel MEG/EEG signals is related to the nature of propagation of an electromagnetic field. The fact is, noninvasive methods of magneto- and electroencephalography do not provide access to the sources of neuronal activity, but represent an instantaneous linear superposition of the activity of several sources [64, 65]. In other words, several sensors can simultaneously reflect the activity of a single source. This effect is called 'bulk conductivity'. In addition, the activity of the sources undergoes a distortion as it propagates through the skull bones, the skin, and other conductive media that can be regarded as low-frequency filters. As a result, the recorded signals from a source of neuronal activity become 'smeared' in space (the field propagation problem) which causes the appearance of false correlations between signals registered by closely located sensors and significantly complicates the interpretation of the reconstructed functional relationships. The bulk conductivity problem deserves close attention and has been considered in a number of reviews [57, 66]. There are several approaches to compensate for the effect of bulk conductivity.

The first and simplest method is to use communication metrics taking no account of the contribution of instantaneous correlation, i.e., introducing no appropriate delay (0 or 180°). This is possible with the help of such functional coupling metrics as the weighted phase lag index [67], the imaginary part of coherence [68], and the phase slope index [69]. In the case of analysis of effective connections, it corresponds to the consideration of an additional 'instantaneous' component in the vector autoregressive model [70, 71]. This method is rather effective, since it disregards the effect of the simultaneous appearance of the field from a single source on several sensors and the corresponding false connections.

The second method is the transition from the reconstruction of connections at the sensor level to that at the source level. In this case, the problem of bulk conductivity disappears by itself in a natural way, but the analysis of connections becomes much more complicated by the appearance of an additional stage of data processing associated with the reconstruction of sources of neuronal activity (this approach is described in detail in Section 2.2).

The third method for the suppression of the bulk conductivity effect is a correct consideration of altered functional connections, i.e., a change in the functional connection metric under the conditions of a given experiment or two different experiments as compared with that in the background conditions. This strategy is based on the fact that the bulk conductivity effect similarly manifests itself under different experimental conditions; therefore, correct 'subtraction' allows false connections to be suppressed.

2.1.2 Signal-to-noise ratio. An important factor that can significantly affect the assessment and subsequent interpretation of functional connections can be a problem related to the noise level in the experimental signal being analyzed and its ratio to the useful component. The problem arises because the recorded signal always contains a noise component originating from measurement and recording errors, as well as from random processes generated by the brain's neuronal ensemble; hence, the difficulties encountered in the evaluation of functional connections in a pair of signals differing in the level of signal-to-noise ratio due, for example, to different impedances of the electrodes in the case of EEG recording. Also, a change in the useful signal-to-noise ratio during the experiment can lead to the appearance of false differences when comparing functional connections under different conditions. This issue is discussed at greater length in Ref. [57] as exemplified by the assessment of the directionality of connections for two different model signals using the Granger causality method.

2.1.3 Problem of statistical significance of connections. Modern neuroimaging technologies permit us to represent brain activity with high spatial and temporal resolution. The specificity of designing and conducting neurophysiological experiments makes the analysis of these data multifactorial, since it implies taking account of different experimental conditions in which they were obtained. Therefore, determining characteristics of brain activity associated with concrete effects or conditions can be a very nontrivial task. The main difficulty in this case is finding the correction due to the multiple comparison problem (MCP) that appears when it is necessary to build a family of statistical inferences. There are traditional conservative methods to address this problem, such as the Bonferroni correction, which consists of lowering the critical level $p_B = p_{cr}/N$, where N is the number of comparisons, p_{cr} is the selected value of the critical level (usually 0.05), and p_B is the value of the critical level taking into account the Bonferroni correction. It is clear that the Bonferroni correction makes it possible to eliminate the influence of the effect of multiple comparisons when their number is small ($N < 10$) and becomes weakly applicable when a large number of hypotheses are tested simultaneously.

Such a situation naturally arises when comparing experimental results in the frequency, space, and time domains that, as a rule, contain a large number of data pairs for comparison ($N \gg 10^2$). To analyze spatial-frequency-temporal characteristics of neuronal activity, more advanced and efficient methods using the nonparameteric cluster-based permutation test have been developed [63]. The main purpose of such statistical testing is to rule out areas (or clusters) of frequency, spatial, or temporal distribution in which significant changes in the measurement data under different experimental conditions were determined inadvertently. Such analysis is aimed at reducing the probability of a type I error, i.e., the number of false positive results.

The problem of correct statistical testing, taking into account the correction due to multiple comparisons, is especially relevant with respect to results of the assessment of functional connections. Specificity of the solution of this problem is first of all determined by the necessity to identify 'clusters'. The authors of a recent study [72] proposed and described in detail a new correct approach to the statistical analysis of the difference in functional relationships under two different experimental conditions that is actually an extension of the nonparametric cluster analysis. An advantage of this approach is it simultaneously reveals significant differences between functional connections in the frequency, temporal, and spatial domains.

2.2 Reconstruction of brain sources to assess connections

The field propagation problem mentioned in Section 2.1.1 arises from the fact that the same area of brain activity is usually recorded by several neighboring sensors at a time which limits the possibilities for the practical use of various functional connectivity measures in the brain calculated at the

sensor level, i.e., based on the signals recorded during EEG or MEG. The field propagation problem significantly complicates correct interpretation of the results. An analysis of neuronal interactions in the space of activity sources in the brain, characteristics of which (position and power) can be reconstructed by special methods based on solving the so-called inverse problem [65, 73], allows an effective solution to this problem. Another important reason for the transition into the source space when assessing connections is the ability to determine the real anatomical location of the interacting brain regions. Here and hereinafter, sources are understood to be the sources of neuronal activity in the brain.

Methods for the location (reconstruction) of sources are constantly being improved, which makes it possible to directly assess the activity of neuronal sources that generate signals observed at the sensor level and facilitates solving the field propagation problem.

In this section, we briefly consider the general principle of reconstruction of neural activity sources and specific features of their use for the assessment and analysis of connections in the source space. Most source-level analytical methods are implemented in two stages.

(1) Assessment of the activity of neuronal sources in the brain from signals recorded at the sensor level by solving the inverse problem. The main classes of these methods are briefly discussed below.

(2) Calculation of connections between recovered sources, which is usually limited to a set of predefined areas of interest in the brain.

A notable exception to the above two-step approach is dynamic causal modeling [74]. This approach is described in more detail below.

2.2.1 Source reconstruction methods. The existing approaches to the reconstruction of neural activity sources make it possible to achieve a spatial resolution of functional brain imaging comparable to that of fMRI and positron emission tomography (PET). With a known set of MEG or EEG signals from an array of external sensors, the inverse problem reduces to the assessment of the properties of current sources inside the brain that generate these signals. First of all, it is necessary to solve the direct problem within which the potentials and external fields on the scalp are calculated for a given set of neuronal current sources. Note that the characteristic frequencies of MEG and EEG signals are, as a rule, below 1 kHz, and most studies consider a frequency range from 0.1 to 100 Hz. As a consequence, the physical processes of propagation of electromagnetic fields resulting in the observed MEG or EEG signals can be described using the quasi-static approximation of Maxwell's equations [75].

Equivalent current dipoles or multipoles are used as source models to solve direct and inverse problems [75, 76]. It is important to note that neuronal activity does not consist of discrete sets of current dipoles. They are just a convenient representation of the coherent activation of a large number of pyramidal cells that can extend over several square centimeters of gray matter. In other words, a current dipole is the most highly sought model in work with MEG and EEG data, since a primary current source of arbitrary length can always be broken into small fragments, each represented by an equivalent current dipole.

Calculating scalp potentials and induced magnetic fields requires solving the direct problem for a given source model. When surface integrals are calculated over realistic head shapes, the corresponding equations are solved numerically. However, there are analytical solutions for simplified geometry, such as that of the human head considered to be made up of a set of nested concentric uniform spherical shells representing the brain, skull, and scalp [77, 78]. For a more accurate solution to the direct problem, anatomical information obtained from high-resolution volumetric images of the brain (using, for instance, MRI or X-ray computed tomography) should be used to determine the surface boundaries of the brain, skull, and scalp from these images [79]. The surfaces found can then be used to calculate direct fields by the boundary element method or the finite element method [80]. Note that one of the most popular head models in MEG studies is the semi-realistic single-shell model proposed in [81], which is characterized by an optimal ratio of accuracy and computational complexity.

There are two classes of methods for the assessment of sources from EEG and MEG data (i.e., for the solution to the inverse problem): parametric and visualizing (nonparametric) [75, 82–84]. In parametric methods, it is assumed that the sources can be represented by several equivalent current dipoles with unknown coordinates and moments determined by nonlinear numerical methods. Nonparametric methods are based on the assumption that the primary sources are intracellular currents in the dendritic trunks of cortical pyramidal neurons aligned normally to the surface of the cortex. In other words, a separate current dipole is assigned to each of the several tens of thousands of elements of the division (tessellation) of the cerebral cortex surface, while the orientation of the dipole is determined by the local normal to the surface. The inverse problem in this case is linear, since the only unknowns are the amplitudes of the dipoles in each element of the partition.

Figure 2 presents an example of the reconstruction of the activity of sources in the cerebral cortex by the method of dynamic visualization of coherent sources [85] from the MEG data (306 channels) recorded in a subject who perceived a Necker cube blinking at a frequency of 6.67 Hz [86]. The result was obtained using the FieldTrip software package [87] in the frequency range determined by the doubled cube blinking frequency: 13.33 ± 2 Hz. Excitation of the primary visual cortex and the visual association area was observed.

Note that the above description of the general approach to reconstructing neural activity sources in the brain does not pretend to be complete; it is only a brief introduction to this issue necessary to disclose the main topic of the review. A detailed discussion of the methods for reconstructing the sources can be found in Refs [75, 82].

To implement the second step of the approach to the analysis of connections at the source level (the reconstruction of connections between localized sources), connectivity measures analogous to those used at the sensor level are employed. A detailed discussion of various connectivity measures is given in Section 2.3.

Note that the dynamic modeling of causality is conceptually different from the methods discussed above [74]. It aims to build a biophysically plausible generative model of the measured data that describes how an input signal activates the system of predetermined interconnected neuronal populations to generate an output signal similar to the measured one. Unlike two-stage methods, the dynamic modeling of causality does not permit calculating parameters of neural activity sources separately but ensures

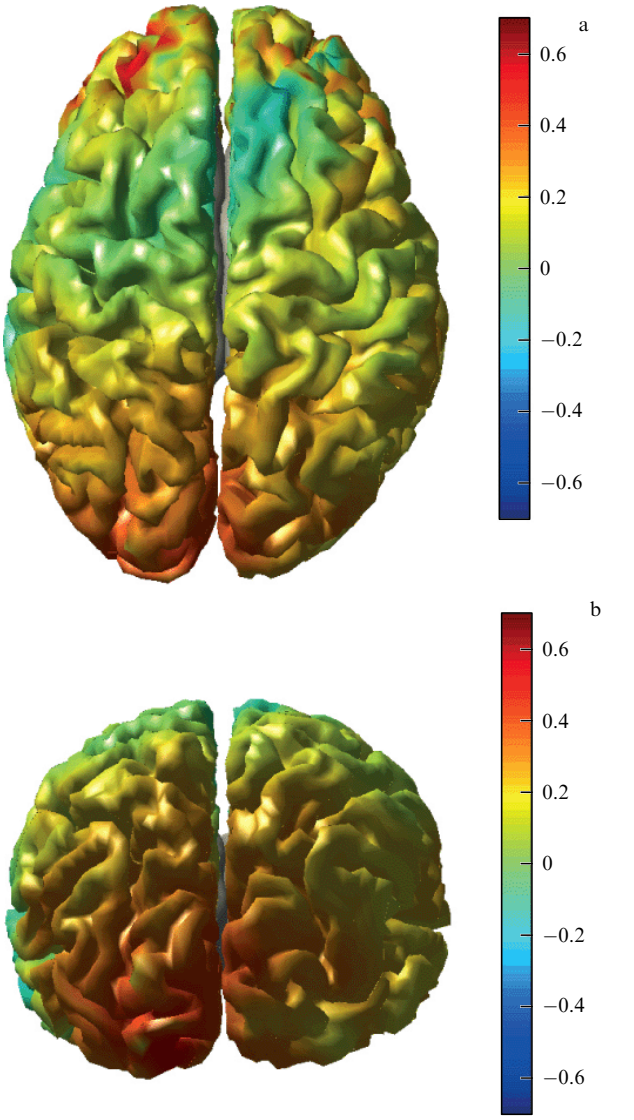

Figure 2. (Color online.) Distribution of normalized changes in the power of sources in the cerebral cortex relative to its background activity during visual processing associated with the perception of a blinking Necker cube: (a) top view, (b) view from the occipital region of the brain. The result was obtained by the method of dynamic visualization of coherent sources using registered MEG data (306 channels).

evaluation of the parameters of connections and sources in a single step [88–91].

2.2.2 Defining areas of interest. Almost all methods for the analysis of functional connectivity between sources allow calculating the connectivity measures between each pair of selected areas of interest or between several areas of interest and the rest of the brain. Obviously, the choice of the areas of interest is a critical step, since the quality of the time series obtained in them determines the accuracy of the analysis of connections between them. Thus, the incorrect choice of the areas of interest can lead to an erroneous result. Let us consider a few strategies for identifying areas of interest.

(1) *Pre-selection* (*a priori selection*). The areas of interest can be selected based on *a priori* information about their involvement in the performance of a certain experimental task (for example, using results of preliminary functional visualization) [85, 92–95]. The *a priori* selection permits us to calculate connectivity measures between all possible pairs of the areas of interest. However, their location may prove suboptimal, or some important areas may be overlooked.

(2) *Assessment of cortico-peripheral coherence*. This strategy is based on the estimation of coherence between peripheral physiological signals and brain activity reconstructed on a discrete grid. Such an estimation allows identifying areas of the brain in which the activity is modulated by the rhythmic processes of peripheral signals. Evaluation of cortico-peripheral coherence can be used, for example, with vibrational components arising during movements and recorded using electromyography (EMG) and tracking devices [85, 95–101]. Brain regions showing maximum cortico-peripheral coherence can serve as reference areas in the analysis of cortical-cortical connections.

(3) *Assessment of coherence at the sensor level*. Gross et al. [85] demonstrated the use of data about coherence between all sensor combinations for an MEG system with planar gradiometers and found coherence between far regions. The respective sources were localized by an iterative procedure. In all likelihood, however, this strategy can not be properly implemented in the majority of cases in view of the field propagation problem.

(4) *Constructing power maps*. One of the most widely used strategies is the choice of the areas of interest based on neuronal activity maps. Brain regions showing the most intense activity during the performance of an experimental task or the greatest difference in the activity under different experimental conditions are selected for a further analysis of connections. This approach was proposed in Ref. [102], where minimum norm estimates were used to reconstruct the time series of sources from nonaveraged data. The most activated regions were identified using surrogate data. To reduce the number of active elements to be considered in the brain volume (voxels), an iterative procedure was used. After the final set of voxels was collected, phase locking was analyzed. This approach was further developed for use in experiments with multiple fragments of brain activity records [74]. A similar method was applied in a study of visual-motor connections [100].

(5) *Methods based on the calculation of coherence*. In Refs [103, 104], an approach was proposed to identify strongly connected areas of the brain based on the calculation of the density of connections over the entire brain. The density of connections for a given voxel was determined as the number of long-range connections exceeding a given coherence threshold. A connectivity density map can be constructed taking into account the coherence threshold, and regions of local maxima on it can be selected as areas of interest. Changes in the density map under various experimental conditions can be analyzed to identify changes in the connections associated with the performance of a specific task.

Ideally, it is possible to disregard any threshold values and calculate connections between all possible combinations of voxels. However, even voxels of moderate size tend to produce several million combinations, which complicates the calculation and interpretation of the resulting connectivity matrices.

In Ref. [105], a computationally efficient algorithm for post-processing of voxel correlation matrices based on a singular-value decomposition is proposed. The sources were reconstructed by the minimum norm estimation method. The calculation of singular-value decomposition of a very large correlation matrix for the sources was reduced to calculating

the singular-value decomposition of the inverse operator that maps signals coming from the sensors into the source space. The sources of neural activity, the first eigenvector of which exceeded some predetermined threshold value, were identified as correlated areas. The proposed method is efficient since it does not rely on *a priori* information, nor does it directly use the activity of the sources. Nevertheless, the choice of the number of relevant eigenvectors and their threshold value, as well as a restriction on the orthogonality of the singular-value decomposition method, is often problematic and depends on the experience and intuition of the researcher.

2.2.3 Limitations and features. Interpreting the results of a connectivity analysis at the level of neural activity sources is complicated by field propagation effects. This is true regardless of the connectivity measure used if its calculation is preceded by the application of the 'traditional' inverse method. By traditional inverse methods are meant those that do not explicitly distinguish between 'interactions' due to the field propagation and real interactions between the sources. These approaches include ray methods, distributed source models, and dipole fitting approaches [75, 82].

The authors of Refs [106, 107] proposed two effective methods aimed at eliminating the influence of the field propagation effect before the solution to the inverse problem. One of these methods uses the imaginary part of the cross-spectral density matrix at the sensor level to identify spatial topographies of the pairs of interacting neuronal sources [107]. The application of an additional minimum overlap constraint permits us to locate interacting sources. The use of the imaginary part of the cross-spectral density guarantees that the interaction cannot be explained by the field propagation effect [68]. The authors of [106, 107] succeeded in locating μ-rhythm and parieto-occipital α-rhythm 'generators' using the EEG data set.

Another method is based on the decomposition into independent components of the residuals of a multivariate autoregressive model fitted to the sensor level data after an initial analysis of the principal components [106]. The residuals of the fitted autoregressive model reflect zero-lag interactions between sensors and, indirectly, between the underlying sources. These zero-delay interactions are a consequence of the field propagation effect. A subsequent analysis of the independent components separates the residuals into a set of statistically independent time series. It is assumed that these components are the residuals of the source-level autoregressive model. The mixing matrix of the independent components contains the topography of interacting sources and can be used to determine their location. This approach was applied to EEG data to identify directed connections of an oscillatory network in the α-frequency range.

Thus, the combined use of methods for the location of neural activity sources and a connectivity analysis based on the reconstructed data on their dynamics opens up prospects for studying transient interactions between brain regions, including the nature of these interactions and their direction [108–112]. Nevertheless, an analysis of connectivity at the source level is far from trivial; caution is needed when interpreting its results [113]. Special attention should be given to the following issues.

(1) An analysis of connections at the source level allows, to some extent, a solution to the field propagation problem.

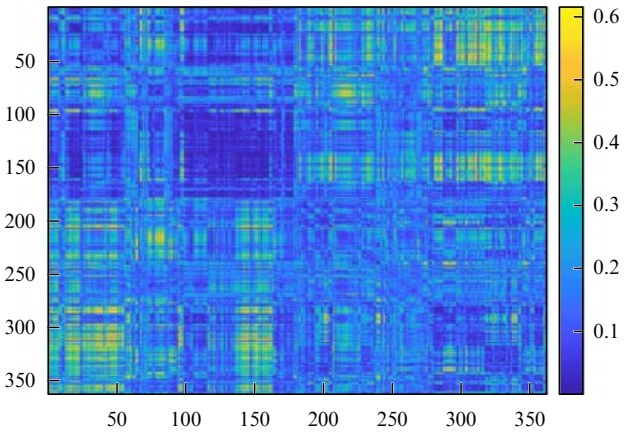

Figure 3. (Color online.) Connectivity map produced using data on reconstructed sources for an experiment with the perception of a blinking Necker cube. The sources were reconstructed from the registered MEG signals. To construct the map, the multimodal cerebral cortex parcellation scheme proposed in [116] was used. Connectivity strength values correspond to the color scale.

However, it does not provide a perfect solution. It is necessary to carry out a quantitative assessment of field propagation based on the results of a source-level reconstruction of connections. This step usually includes the use of estimates of spatial inhomogeneity of the reconstructed sources [114, 115]. Moreover, it is necessary to regularly analyze power variations under changing conditions and take them into consideration when interpreting the results.

(2) The choice of the areas of interest often requires either an interaction with the user or the involvement of some arbitrary parameters. Ideally, the use of any *a priori* information for the choice of areas of interest should be replaced by an estimation of the connectivity among all possible combinations of voxels.

Figure 3 presents an example of a connectivity map constructed using the FieldTrip software package [87] based on data on reconstructed sources for an experiment with the perception of a blinking Necker cube. The sources were reconstructed from recorded MEG signals (see Fig. 2). Due to the initially large number of dipole sources (more than 8,000), the resulting matrix contains over 64 million elements, which makes it uninterpretable. The most effective strategy for reducing the connectivity matrix dimension is the use of brain parcellation. Such diagrams are usually built on the basis of anatomical information about the human brain or modalities. Then, the connections are assessed between the brain regions for a given parcellation scheme rather than between individual dipole sources. To build the map shown in Fig. 3, the multimodal cerebral cortex parcellation scheme proposed in [116] was used; it contains 180 regions for each hemisphere. The imaginary part of coherence was used as a connectivity measure, which made it possible to effectively suppress parasitic coherence caused by the propagation of an electromagnetic field [68].

2.3 Hierarchy and classification of the methods for reconstructing functional connections

Let us briefly consider the classification and hierarchy of the most frequently used effective measures for assessing functional connections (Fig. 4). First, all methods can be divided in terms of applicability for determining the direction of

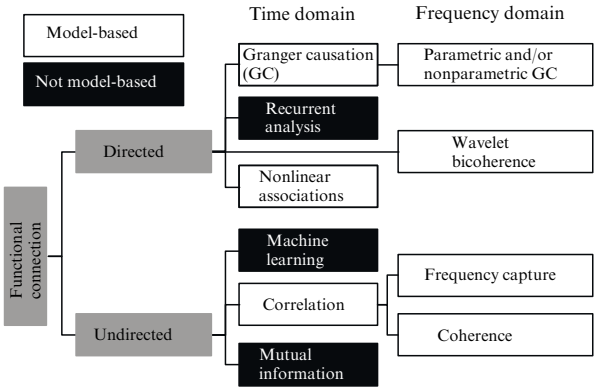

Figure 4. Classification of methods for the assessment of functional connections.

interaction. The undirected methods tend to assess the magnitude of the interdependence between signals without reference to the direction of exposure. Conversely, the directed methods presuppose the determination of statistical causality when, for example, in the case of Granger causality, it is possible to predict the behavior of one signal from that of another; hence, the possibility of identifying causal (directed) connections.

Within the framework of both directed and undirected methods for the assessment of functional connections, a distinction can be made between model-dependent and model-independent approaches. As a rule, model-based approaches (shown in white in Fig. 4) assume linear interactions between two signals. The simplest measure for undirected model interactions is Pearson's correlation coefficient, which characterizes the linear dependence between two random variables (see Section 2.3.1). Another model-based approach allowing evaluation of nonlinear interactions makes use of methods for synchronizing two signals that, despite the convenience and simplicity of interpretation, do not permit assessing the directionality of connections (see Section 2.3.2). A more general approach that does not imply linear relationships is the mutual information method (see Section 2.3.3) measuring the generalized (linear and nonlinear) interdependence between two or more time series based on information theory. The mutual information method belongs to the class of model-independent approaches (see black boxes in Fig. 4 and Section 2.3.3). Convenient methods for the assessment of the functional dependence, not based on models either, are the recurrent method and the method using a universal approximator (a feedforward artificial neural network) that actually makes it possible to reveal generalized synchronization between two processes (see Section 2.3.4).

Finally, one can distinguish between functional connectivity measures calculated from the representation of signals in time or frequency domains. To identify individual rhythmic components, it is convenient to consider the frequency-domain representation of the signals. A transformation to the frequency domain can be achieved using nonparametric (Fourier decomposition, wavelet analysis, Hilbert transform) or parametric (autoregressive models) methods. Functional connectivity indicators in the frequency domain can then be used to assess interactions among brain regions. Many of these methods quantify, to one degree or another, the phase coordination between rhythmic components in the signals. The nonrandom distribution of the phase difference may indicate a functionally significant connection between neuronal populations.

Let us consider various methods for evaluating functional and effective connections in more detail.

2.3.1 Linear methods. *Pearson's correlation coefficient*. The simplest and most easily interpreted measure for the assessment of functional connections in the time domain is the Pearson correlation coefficient, which characterizes the linear statistical relationship between two processes. Within the framework of the linear interaction model, the Pearson coefficient shows the fraction of variance of one quantity explained by the dispersion of another and vice versa. Let the time series $X=\{X_1, X_2, \ldots, X_N\}$ and $Y=\{Y_1, Y_2, \ldots, Y_N\}$ represent neural activity recorded by sensors x and y, respectively. Then, the Pearson correlation coefficient is defined as

$$r_{XY} = \frac{\operatorname{cov} XY}{\sigma_X \sigma_Y}, \tag{1}$$

where $\operatorname{cov} XY$ is the covariance of the time series X and Y,

$$\operatorname{cov} XY = \frac{1}{N}\sum_{t=1}^{N}(X_t - \overline{X})(Y_t - \overline{Y}), \tag{2}$$

σ_X, σ_Y and $\overline{X}$, $\overline{Y}$ are mean square deviations and mean values of the time series X and Y.

Independent processes correspond to $r_{XY} = 0$, while $r_{XY} = \pm 1$ indicates a positive (in-phase) or negative (anti-phase) correlation, respectively.

A few important features of the Pearson correlation coefficient as a functional connectivity measure follow from this mathematical definition. First, the Pearson correlation coefficient describes the relationship between two processes from the standpoint of amplitude synchronization. Second, this measure generally evaluates undirected interaction. Third, it does not take into account the temporal structure of the signals under study; in other words, the correlation takes the same value if the time series are randomly mixed. In addition, the assessment of the functional relationship using the Pearson correlation coefficient is most strongly influenced by the bulk conductivity effect, since it reveals instantaneous linear amplitude correlation (see Section 2.1.1).

Some of the above limitations can be taken into account by temporarily shifting one signal relative to another. Let $Y^\tau = \{Y_\tau, Y_{\tau+1}, \ldots, Y_{N+\tau}\}$ represent a time series Y shifted τ time counts to the left with respect to the X series. In this case, the Pearson correlation coefficient is a function of the time shift:

$$r_{XY}(\tau) = \frac{\operatorname{cov} XY^\tau}{\sigma_X \sigma_{Y^\tau}}. \tag{3}$$

Consideration of the dependence of the Pearson correlation coefficient on the time shift allows taking into account the temporal structure of the data and drawing conclusions about the direction of the analyzed functional connection. Note that the presence of a maximum of this dependence at $\tau > 0$ indicates that process X affects Y ($X \rightarrow Y$); conversely, process Y affects X ($Y \rightarrow X$) when the maximum is at $\tau < 0$. It is important that an analysis of the linear correlation of time series shifted in time with respect to each other make it possible to eliminate the influence of the bulk conductivity effect, since it excludes the instantaneous correlation ($\tau = 0$),

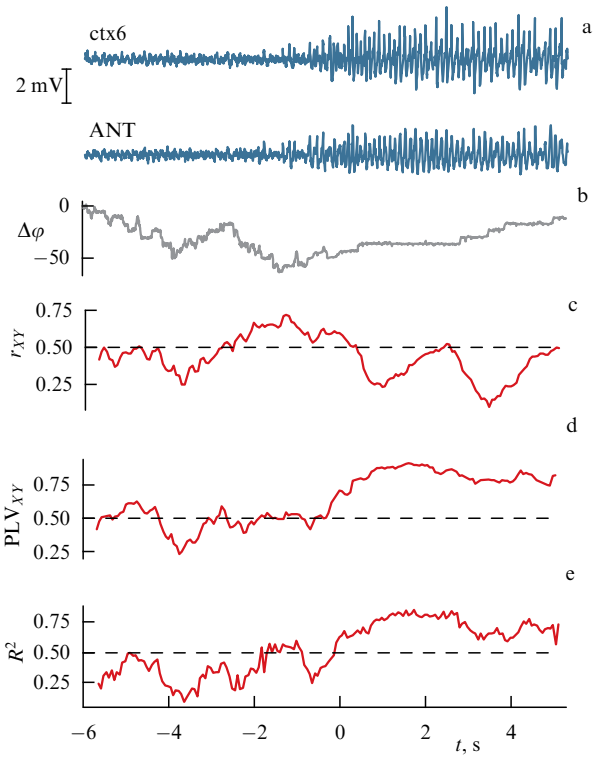

Figure 5. Illustration of the calculation of various functional connection measures for signals from the thalamo-cortical network of the brain of a WAG/Rij rat during a seizure of absence epilepsy [117]. (a) Invasive recordings of electrical activity from the 6th cortical layer and the thalamic ANT nucleus between which the functional connection was assessed. (b) Phase difference between ctx6 and ANT signals obtained using the Hilbert transform (9)–(11). Variations in the functional connection in time calculated using Pearson's linear correlation coefficient r_{XY} (1) (c), phase locking measure PLV_{XY} (12) (d), and generalized synchronization method with machine learning-based detection (e). Calculations were carried out in a 2-s-wide movable window.

which can be falsely caused by field propagation from one of the sources.

Figure 5a illustrates the results of the calculation of functional connections as exemplified by a pair of signals from the thalamo-cortical network of the brain in WAG/Rij rats during the formation of an episode of absence epilepsy. The calculation is based on the experimental data from our work [117] and provide a good example of the methods for analyzing functional connections, because this type of epilepsy is characterized by enhanced synchronization of the neuronal activity in the cortex and thalamic nuclei, as opposed to that during normal activity (Fig. 5b).

Figure 5c shows a change in functional connectivity calculated based on the Pearson coefficient (1). It can be seen that a linear analysis reveals an increased correlation 2 s before the attack and a sharp decrease in the linear correlation coefficient during the seizure. This suggests that a linear analysis is not suitable for studying the spike activity when the interaction between brain regions is essentially nonlinear.

Coherence. Pearson's correlation coefficient is a linear measure of functional connectivity in the time domain. A widely used equivalent measure for quantifying phase synchronization in the frequency domain is the coherence coefficient [59, 96–98, 118, 119] (some authors prefer the term magnitude squared coherence).

To begin with, let us represent X and Y signals in the frequency domain using the Fourier transform:

$$S_X(\omega) = \int_{-\infty}^{\infty} \mathrm{d}t\, X(t) \exp(-\mathrm{i}\omega t) = A_X(\omega) \exp\left(-\varphi_X(\omega)\right), \quad (4)$$

$$S_Y(\omega) = \int_{-\infty}^{\infty} \mathrm{d}t\, Y(t) \exp(-\mathrm{i}\omega t) = A_Y(\omega) \exp\left(-\varphi_Y(\omega)\right),$$

where $S_{X,Y}(\omega)$ are the complex Fourier spectra of signals X and Y, respectively, $A_{X,Y}(\omega)$ and $\varphi_{X,Y}(\omega)$ are the amplitudes and phases of signals X and Y being analyzed. Then, the coherence coefficient is calculated as

$$\mathrm{coh}_{XY}(\omega) = \frac{\left|A_X(\omega)A_Y(\omega)\exp\left[\mathrm{i}\left(\varphi_X(\omega) - \varphi_Y(\omega)\right)\right]\right|}{\sqrt{A_X^2(\omega)A_Y^2(\omega)}}. \quad (5)$$

Here, the numerator is the cross-spectral density of signals X and Y at frequency ω and the denominator is the square root of the product of the spectral powers of X and Y at frequency ω. According to the above mathematical definition, the coherence coefficient varies from 0 to 1: $\mathrm{coh}_{XY}(\omega) = 0$ corresponds to the absence of correlation at ω and, on the contrary, $\mathrm{coh}_{XY}(\omega) = 1$, to complete correlation.

2.3.2 Nonlinear methods. Linear methods of analysis of functional connections described in Section 2.3.1 allow us to obtain an unambiguous and correctly interpreted result only for the linear relationship between the signals under investigation. As a rule, neuronal interactions are nonlinear, and a family of *nonlinear* methods has been developed to overcome this limitation. The most popular and frequently used ones are discussed below.

Nonlinear associations. A method for evaluating nonlinear associations was proposed by the authors of [120, 121] as a generalization of the linear correlation analysis. Let us consider, without the loss of generality, the amplitude of signal Y versus the amplitude of signal X. The expectation of Y based on the known X value is expressed analytically as

$$\mu_{Y|X}(X) = \int_{-\infty}^{\infty} Yp(Y|X)\,\mathrm{d}Y; \quad (6)$$

in this case, the dependence given by relation (6) is a regression curve, and the nonlinear association measure η^2 is calculated as

$$\eta_{XY}^2 = \frac{\sigma_{Y\mathrm{t}}^2 - \sigma_{Y\mathrm{un}}^2}{\sigma_{Y\mathrm{t}}^2}, \quad (7)$$

where $\sigma_{Y\mathrm{t}}^2$ is the total variance of Y, and $\sigma_{Y\mathrm{un}}^2$ is the 'unexpected' variance of Y. The latter is calculated as the difference between the total variance of Y and the expected variance of Y obtained from the regression curve.

Unlike the linear correlation coefficient, which is symmetric, i.e., $r_{XY} = r_{YX}$, the nonlinear association measure may turn out to be asymmetric, $\eta_{XY}^2 \neq \eta_{YX}^2$. This property is of interest and importance from the standpoint of analysis of the nature of interaction between X and Y. If the relationship between the signals is linear, then η_{XY}^2 approximates the Pearson correlation coefficient r_{XY}^2 and, accordingly, is symmetric. In the case of a nonlinear but one-to-one correspondence between X and Y, the asymmetry turns out

to be slight. Marked asymmetry of the nonlinear association measure is observed in the case of a nonlinear and ambiguous relationship between X and Y. By analogy with the correlation coefficient, one can introduce a time shift between the signals under study to estimate the directionality of the connection and make this metric more resistant to the bulk conductivity effect.

Phase lock measure. A mathematical concept of importance for constructing nonlinear methods to assess functional connections is chaotic synchronization [122, 123]. Numerous studies in the field of neuroscience show that the phase of a signal as its temporal characteristic can often turn out to be more informative than its amplitude, due to the corresponding changes in synchronicity. This type of synchronization in which the capture of phases of oscillatory neuronal activity is observed is termed phase synchronization [124–127].

One of the most popular metrics for assessing phase synchronization in neuroscience is the phase locking value (PLV) [128]. This measure is based on the fact that, during phase locking, the phase difference between the two signals, X and Y, remains constant in the absence of amplitude correlation, which is mathematically expressed as

$$\left|\varphi_X(t) - \varphi_Y(t)\right| \approx \text{const}\,. \tag{8}$$

To isolate the phase dynamics of a signal, the analytical signal concept is often used [129]:

$$H(t) = X(t) + \mathrm{i}\tilde{X}(t)\,, \tag{9}$$

where $X(t)$ is the initial signal, and $\tilde{X}(t)$ is its Hilbert transform defined in the sense of principal value (v.p.) of the Cauchy integral:

$$\tilde{X}(t) = \frac{1}{\pi}\,\text{v.p.}\int_{-\infty}^{\infty}\frac{X(t')}{t-t'}\,\mathrm{d}t'\,. \tag{10}$$

The analytical signal phase is defined as

$$\varphi_X(t) = \arctan\frac{\tilde{X}(t)}{X(t)}\,, \tag{11}$$

and the measure of phase capture of two signals, X and Y, having phases φ_X and φ_Y is calculated according to the following expression:

$$\text{PLV}_{XY}(t) = \left|\frac{1}{N}\sum_{t=1}^{N}\exp\left[\mathrm{i}\big(\varphi_X(t) - \varphi_Y(t)\big)\right]\right|. \tag{12}$$

PLV_{XY} was found to lie in the range from 0 to 1, where 1 characterizes exact phase synchronization and 0 means complete independence of the phases of the signals under consideration. Compared to the coherence measure coh_{XY}, the phase capture measure PLV_{XY} provides a more accurate result and requires fewer computational resources and fewer data for a given temporal resolution. Moreover, the phase capture measure is an optimal choice in an analysis of nonstationary signals.

The evaluation of functional connectivity using the phase capture measure is exemplified in Fig. 5d. The corresponding phase difference calculated using the Hilbert transform is shown in Fig. 5b. In contrast to the Pearson linear correlation index r_{XY}, PLV_{XY} increases sharply after the onset of an attack of absence epilepsy, demonstrating strengthening of the nonlinear interaction from the perspective of phase synchronization of neuronal activity in the thalamo-cortical network of the brain.

A similar analysis of phase locking was carried out in connectivity studies at the source level in addition to the traditional analysis of coherence [95, 100, 103]. Both coherence and phase lock measures are symmetric; therefore, they do not allow the directionality of connections between interacting signals to be assessed. However, time delays can be estimated from the phase slope of the cross-spectrum of the time series of interest [130, 131].

Phase lag index. In addition to the traditional measures for the assessment of phase synchronization developed in physics (e.g., in the theory of chaotic oscillations), new approaches to the analysis of functional connectivity have recently been proposed based on the temporal dynamics of signal phases. The elaboration of new approaches is motivated by the necessity to interpret the results obtained by traditional methods subject to the effects described in Section 2.1. In what follows, we consider an increasingly popular functional coupling metric, the phase lag index (PLI) [132], which takes into account a number of the previously mentioned problems and limitations.

The main purpose of using the phase lag index is to assess phase synchronization while eliminating problems related to bulk conductivity and changes in the impedance of the electrodes (in the case of EEG recording). This can be achieved by disregarding the phase differences concentrated around values that are multiples of π: 0, π, 2π, 3π, etc. One of the ways is to introduce a certain asymmetry index for the phase difference distribution in the vicinity of zero; in the absence of coupling between the signals, the distribution is uniform and symmetric, whereas any deviation from symmetry serves as an indicator of the coupling. Here, asymmetry means that the probability of finding the phase difference in the interval $-\pi < \varphi_X - \varphi_Y < 0$ differs from that in the $0 < \varphi_X - \varphi_Y < \pi$ range. Such asymmetry implies the presence of a nonzero phase difference (or delay), the nature of which is unrelated to the neural activity source common to the two signals due to the simultaneous observation of the bulk conductivity effect on the neighboring electrodes.

The phase lag index characterizing asymmetry of the phase difference distribution is defined as

$$\text{PLI}_{XY} = \left|\left\langle\text{sign}\big(\varphi_X(t) - \varphi_Y(t)\big)\right\rangle\right|, \tag{13}$$

where the operator $\langle\ldots\rangle$ means time averaging. Note that expression (13) requires that the phase difference be determined within the $[-\pi, \pi]$ interval. If it is determined in the $[0, 2\pi]$ interval, the expression for the evaluation of PLI should be presented in the form

$$\text{PLI}_{XY} = \left|\left\langle\text{sign}\big(\sin\left[\varphi_X(t) - \varphi_Y(t)\right]\big)\right\rangle\right|. \tag{14}$$

In accordance with (13) and (14), PLI was found to lie in a range from 0 to 1, where 1 corresponds to an ideal phase capture other than a multiple of π, and 0 indicates the complete absence of connectivity. It is also important that the phase lag index (PLI) in this definition not provide information on the directionality of the connection, i.e., which of the two signals has a leading phase. This problem can be solved by excluding the modulus from expressions (13) and (14).

An alternative way to assess functional connections between signals from short time series is provided by the wavelet bicoherence method [133, 134], which finds application in the study of cognitive processes and the processing of stimulus information (see, for instance, [135–137]).

2.3.3 Evaluation of functional connectivity based on mutual information. Mutual information characterizes the amount of data on the state of a system derived from a dataset on the state of another system [138]; it allows us to reveal linear and nonlinear dependences between the time series or neuronal sources of interest [139, 140]. If only the state of system X is known, it is possible to estimate the average amount of information about its state or entropy:

$$H(X) = -\sum_{t=1}^{N} P_X(X_t) \log_2 P_X(X_t)\,, \tag{15}$$

where $P_X(X_t)$ is the probability of X taking the value X_t. This value also has the meaning of the uncertainty of observing state X. If at the same time process Y takes place that assumes state Y_k, then the definition of the conditional probability should be used and expression (15) presented in the form of conditional entropy:

$$H(X|Y = Y_k) = -\sum_{t=1}^{N} \frac{P_{XY}(X_t, Y_k)}{P_Y(Y_k)} \log_2 \frac{P_{XY}(X_t, Y_k)}{P_Y(Y_k)}\,. \tag{16}$$

Here, $P_{XY}(X_t, Y_k)$ is the joint probability that $X = X_t$ while $Y = Y_k$. The quantity $H(X|Y = Y_k)$ characterizes the uncertainty of state X at a known value $Y = Y_k$. From here, one can find the average uncertainty of state X over all known Y values:

$$\begin{aligned} H(X|Y) &= \sum_{k=1}^{N} P_Y(Y_k) H(X|Y = Y_k) \\ &= -\sum_{k=1}^{N}\sum_{t=1}^{N} P_{XY}(X_t, Y_k) \log_2 \frac{P_{XY}(X_t, Y_k)}{P_Y(Y_k)} \\ &= H(X, Y) - H(Y)\,, \end{aligned} \tag{17}$$

where

$$H(X, Y) = -\sum_{k=1}^{N}\sum_{t=1}^{N} P_{XY}(X_t, Y_k) \log_2 P_{XY}(X_t, Y_k)\,. \tag{18}$$

Since $H(X)$ is the *a priori* uncertainty of state X, and $H(X|Y)$ is the a posteriori uncertainty at known Y values, the fraction of state X uncertainty reduced by virtue of information about state Y can be expressed as

$$\begin{aligned} I_{XY} &= H(X) - H(X|Y) = H(X) + H(Y) - H(X, Y) \\ &= -\sum_{k=1}^{N}\sum_{t=1}^{N} P_{XY}(X_t, Y_k) \log_2 \frac{P_{XY}(X_t, Y_k)}{P_X(X_t) P_Y(Y_k)}\,. \end{aligned} \tag{19}$$

The quantity I_{XY} is called cross-mutual information [141]. If processes X and Y are completely independent, then $P_{XY} = P_X P_Y$; therefore, $I_{XY} = 0$.

For example, the authors of Refs [139, 140] used magnetic imaging as an inverse method [142] to determine the zones of activity in the brain. The areas of interest were determined by identifying coherently activated brain regions. Time series of activity of each area of interest were registered; then, an analysis of mutual information was carried out. Mutual information was calculated between all possible pairs of the areas of interest in a given range of time delays.

It is also important to understand that the mutual information measure is symmetric with respect to directionality $I_{XY} = I_{YX}$; however, the use of signals with time delays can give an idea of the directionality of connections.

2.3.4 Methods based on generalized synchronization. Recently, a few more measures for the assessment of functional connections have been proposed; some of them based on the diagnostics of generalized synchronization deserve special attention [123, 143–146]. Synchronization of this type implies the unambiguous functional correspondence between the states of two related processes:

$$Y(t) = F\big(X(t)\big)\,. \tag{20}$$

Evidently, the limiting case of generalized synchronization is complete synchronization, $Y(t) = X(t)$.

The above mathematical definition of generalized synchronization applies to the case of unidirectional action $X \to Y$. For the mutual connection $X \leftrightarrow Y$, the generalized synchronization criterion is expressed as follows [147]:

$$F\big(X(t), Y(t)\big) = 0\,. \tag{21}$$

From the standpoint of nonlinear dynamics, in the case of generalized synchronization, the trajectory of one system in the space of states is totally determined by the trajectory of the other system and vice versa. To consider the dynamics of systems in the state space based on the known time series, the corresponding phase trajectories $\mathbf{x}(t)$ and $\mathbf{y}(t)$ are reconstructed from the initial signals $X(t)$ and $Y(t)$ using the Takens theorem [148]:

$$\begin{aligned} \mathbf{x}(t) &= \big\{X(t), X(t + l), X(t + 2l), \ldots, X\big(t + (m - 1)l\big)\big\}\,, \\ \mathbf{y}(t) &= \big\{Y(t), Y(t + l), Y(t + 2l), \ldots, Y\big(t + (m - 1)l\big)\big\}\,, \end{aligned} \tag{22}$$

where l is the shift and m is the dimension of the state space. Note that the values of l and m can be chosen either empirically or based on mathematical criteria [149, 150]. The methods allowing an evaluation of the functional connections between X and Y from the recovered trajectories $\mathbf{x}(t)$ and $\mathbf{y}(t)$ are described below.

Recurrent analysis. Recursion or repetition in time is a fundamental property of various natural processes. It means that a given system returns to its earlier states in the course of evolution. The recurrence plot as a method for visualizing a repetition process is a powerful tool for analyzing systems based on time series reflecting their dynamics (see the detailed review by Marwan et al. [151]).

Let $\mathbf{x} = \{\mathbf{x}_1, \mathbf{x}_2 \ldots, \mathbf{x}_N\}$ be a discrete time series; then, the recurrent matrix can be given by the following expression:

$$R_x^{i,j} = \begin{cases} 1 : \mathbf{x}_i \approx \mathbf{x}_j\,, \\ 0 : \mathbf{x}_i \not\approx \mathbf{x}_j\,, \end{cases} \quad i, j = 1, \ldots, N\,, \tag{23}$$

where N is the number of considered states, and $\mathbf{x}_i \approx \mathbf{x}_j$ means the equivalence of states up to an error (distance) ε.

A comparison of recurrent matrices of two processes gives information on the relationship between them. Romano et al. [152] showed that two processes are functionally related (in fact, they are in a generalized synchronization mode) if they have similar recursion maps. Based on this finding, Goswami et al. [153] developed a connectivity measure referred to as the recurrence-based measure of dependence (RMD). This measure characterizes the dependence between the two processes and its direction. Thus, the RMD determines the presence or absence of a causal relationship in a pair of processes in terms of establishing a functional (linear or nonlinear) dependence between them.

For a pair of trajectories, $\mathbf{x}(t)$ and $\mathbf{y}(t)$, the RMD is defined as

$$\mathrm{RMD}_{xy} = \log_2\left(\frac{1}{N}\sum_{t=1}^{N}\mathrm{RMD}_{xy}^{i}\right), \tag{24}$$

$$\mathrm{RMD}_{xy}^{i} = \frac{P(x_i, y_i)}{P(x_i)\,P(y_i)}. \tag{25}$$

The probabilities $P(x_i)$ and $P(y_i)$ as well as the joint probability $P(x_i, y_i)$ are calculated based on the recurrent matrices (23) of the $x(t)$ and $y(t)$ processes:

$$P(x_i) = \frac{1}{N}\sum_{j=1}^{N} R_x^{i,j}, \tag{26}$$

$$P(y_i) = \frac{1}{N}\sum_{j=1}^{N} R_y^{i,j}, \tag{27}$$

$$P(x_i, y_i) = \frac{1}{N}\sum_{j=1}^{N} \mathrm{JR}_{xy}^{i,j}, \tag{28}$$

$$\mathrm{JR}_{xy}^{i,j} = R_x^{i,j} R_y^{i,j}, \tag{29}$$

where JR is the joint recurrent matrix of x and y.

To find the direction of the nonlinear interaction between processes x and y, we introduce the time shift τ into equations (24) and (25):

$$\mathrm{RMD}_{xy}(\tau) = \log_2\left(\frac{1}{N'}\sum_{k=1}^{N'}\mathrm{RMD}_{xy}^{k}(\tau)\right), \tag{30}$$

$$\mathrm{RMD}_{xy}^{k}(\tau) = \frac{P_{xy}(x_k, y_{k+\tau})}{P_x(x_k)P_y(y_{k+\tau})}, \tag{31}$$

where $N' = N - \tau$ and $y_{k+\tau}$ is the trajectory y_k shifted by τ with respect to x_k. The $\mathrm{RMD}_{xy}(\tau)$ dependence has a local maximum $\tau_{xy}^{*} = \mathrm{argmax}[\mathrm{RMD}_{xy}(\tau)]$. The sign τ_{xy}^{*} determines the direction of the connection: process x affects y, if $\tau_{xy}^{*} > 0$, and vice versa. In addition, the value $\mathrm{RMD}_{xy}^{*} = \mathrm{RMD}_{xy}(\tau_{xy}^{*})$ can be used to assess the strength of connectivity between processes x and y.

The recurrent approach has been successfully used to analyze the functional relationship over short biological and climatic time series [16, 25, 153–155]. The advantages of this approach include the possibility of using short time series and revealing nonlinear directed interactions.

Machine learning. A fundamentally different approach to the analysis of functional connections from the standpoint of generalized synchronization was proposed in [117], where the mathematical apparatus of machine learning was used to identify functional dependence (21). To reveal dependences between the behavior of trajectories $\mathbf{x}(t)$ and $\mathbf{y}(t)$, a feedforward artificial neural network (ANN) was used. An ANN is a computing system designed to reveal unknown and usually complex functional relationships between input and output data [156]; therefore, it provides a suitable tool to diagnose generalized synchronization. Indeed, in accordance with the approximation theorem, an ANN with nonlinear functions in hidden layers can approximate any arbitrarily specified function [157, 158]. A nonlinear ANN can also approximate the mapping of functions from one finite-dimensional discrete space to another [156]. This property of ANNs allows approximating the functional relation F in (21), considering only an experimental data set $\mathbf{x}(t_i)$ and $\mathbf{y}(t_i)$, where $t_i = i\Delta t$ is the discrete moments of time and $1/\Delta t$ is the sampling rate.

Figure 6 illustrates schematically the proposed method for detecting functional connections using ANNs. When considering two related processes, the dynamics of which are represented by multidimensional signals (or trajectories in a multidimensional space of states) $\mathbf{x}(t)$ and $\mathbf{y}(t)$, functional connectivity implies $\mathbf{y}(t) = F(\mathbf{x}(t))$. From the mathematical point of view, an ANN is a mapping $f: \mathbf{x} \to \mathbf{y}$; therefore, ANNs can be used to build a model of the unknown ratio $F(\ldots)$ and determine the state y only on the basis of state x. In other words, given that there is a true functional relation $\mathbf{y}(t) = F[\mathbf{x}(t)]$, the ANN can approximate it and give a sufficiently accurate estimate $\mathbf{y}'(t)$ of the $\mathbf{y}(t)$ state based on $\mathbf{x}(t)$. On the contrary, if $\mathbf{x}(t)$ and $\mathbf{y}(t)$ are functionally unrelated, the ANN cannot learn to find a correspondence between states $\mathbf{x}(t)$ and $\mathbf{y}(t)$ and therefore cannot accurately predict the state of the latter system. It can be concluded that the criterion for identifying the functional connectivity is the equality of the predicted actual values of y and those predicted using the ANN: $\mathbf{y}'(t) = \mathbf{y}(t)$.

To train the ANN, a pair of multidimensional time series (trajectories) reflecting the dynamics of interacting systems $\mathbf{x} = \{\mathbf{x}(t_1), \mathbf{x}(t_2), \ldots, \mathbf{x}(t_N)\}$ and $\mathbf{y} = \{\mathbf{y}(t_1), \mathbf{y}(t_2), \ldots, \mathbf{y}(t_N)\}$ can be used. Suppose, without loss of generality, that $\mathbf{x}$ acts on $\mathbf{y}$. Vector $\mathbf{y}(t_i)$ is put in correspondence with each vector $\mathbf{x}(t_i)$; $\mathbf{x}$ and $\mathbf{y}$ stand for input and target data, respectively. The data are normalized in the [0, 1] range, mixed, and divided into training and test sets in equal proportions. To correct the retraining of the model, the discrepancy between the training and validation errors is checked if these values diverge during the last 10 learning epochs; then, the process ends and starts

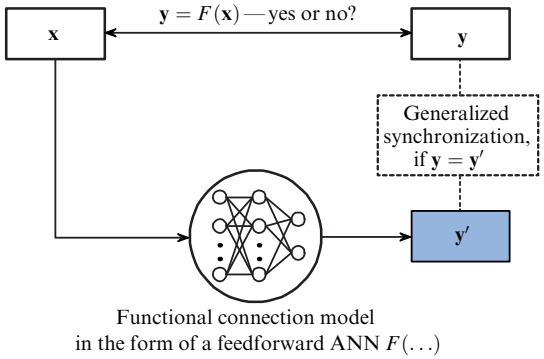

Figure 6. Schematic representation of the method for the assessment of functional connections using a feedforward ANN (modified scheme from Ref. [117]).

anew. To quantify the degree of functional dependence, the coefficient R^2 is used that evaluates the correspondence of the initial $\mathbf{y}(t)$ and output ANN $\mathbf{y}'(t)$ data:

$$R^2 = 1 - \frac{\sum_{d=1}^{D}\sum_{i=1}^{N}\left(\mathbf{y}_d(t_i) - \mathbf{y}'_d(t_i)\right)^2}{\sum_{d=1}^{D}\sum_{i=1}^{N}\left(\mathbf{y}_d(t_i) - \bar{\mathbf{y}}_d\right)^2}\,, \tag{32}$$

where D is the number of measurements of the time series (or the space of states), $\mathbf{y}_d(t)$ and $\mathbf{y}'_d(t)$ are components d of vector $\mathbf{y}(t)$ and its prediction made using the ANN, respectively. R^2 ranges from 0 to 1 and characterizes the amount of data accurately predicted by the ANN. Because $R^2 = 0.5$ indicates that only half of the data is accurately approximated by the model, this value is further considered the threshold accuracy.

The described method tested in an analysis of generalized synchronization in model chaotic systems was used to demonstrate the rearrangement of functional connections in the thalamo-cortical network of WAG Rij rats during an epileptic discharge (the results are described in detail in Section 3.4). An example of the analysis of functional connections using machine learning shown in Fig. 5e demonstrates excellent agreement with the nonlinear PLV_{XY} method based on phase synchronization.

The advantages of the method include the capability to work with short time series and analyze nonlinear connections between interacting processes. In addition, the approach based on the application of machine learning is resistant to noise, which is important in the context of the analysis of functional connections in signals of a biological nature.

2.4 Methods for assessing effective connections

The methods for assessing functional connections discussed in the foregoing assume connectivity between the analyzed brain areas as a certain statistical relationship evaluated by calculating a time series correlation or synchronization that characterize their neural activity. Another equally important concept of brain connectivity analysis is effective connectivity [51]. In the framework of this concept, connectivity is understood as the impact of one neuronal system on another, reflecting the causality of interaction between active brain regions. In other words, connectivity reflects the direction and strength of the information flow between different parts of the brain. In Sections 2.4.1 and 2.4.2, the most extensively used methods for the reconstruction of effective connections are considered.

2.4.1 Dynamic causal modeling. Dynamic causal modeling (DCM) is one of the most widely used methods for the analysis of effective connections [159] that belongs to the class of model-based techniques. The key idea behind the DCM approach is the simulation of the response of a dynamic system in the form of a network of interacting sources of neural activity described by a system of ordinary or stochastic differential equations in the framework of either a neural mass model [91] or a conductivity-based model [160]. Originally, the DMP method was developed to analyze fMRI data; later, it was modified for the treatment of MEG/EEG data [89].

Regardless of the neuroimaging technique, the construction of a phenomenological dynamic model is based on the experimental design, understood as a method of conducting research with the use of suitable tools, a set of stimuli, and information on the mode of their presentation.

As a rule, a neurophysiological experiment is aimed at studying the brain either in the state of activity provoked by the performance of a specific task or in the state of passive rest. In the former case, the reaction of the brain depends on the stimuli controlled by the experimenter. External stimuli control neuronal processes either directly, e.g., through evoked potentials, or by modulating them via the interaction between large neuronal ensembles. In the framework of the model, both mechanisms (external and modulatory) are considered to be separate factors. In the second case, only internal interactions in the neural network of the brain are taken into account.

In general terms, the dynamic model of causality is presented in the following form:

$$\begin{aligned} \dot{z}(t) &= F\left(z(t), u(t), \theta\right), \\ h(t) &= G\left(z(t), \theta\right) + \varepsilon\,, \end{aligned} \tag{33}$$

where $z(t)$ is the function describing the state of the system of neurons at the time point t, $u(t)$ is the external stimulus, θ are the parameters of the model (topology and strength of internode connections), F is the function determining the dynamics of neural processes, $h(t)$ are the signals of neural activity generated and measured during the experiment, G is the function relating dynamics of neural processes to output signals, and ε is the additive measurement noise. Based on (33), the definition of the model consists of setting the functional relations $F(\ldots)$ and $G(\ldots)$ and the choice of 'active' connections in the hypothetical network interaction model.

Several potential models having been identified, and it is necessary to select parameters for each of them. In the framework of the DCM approach, this procedure is carried out using the variational Bayesian methods under the Laplace approximation [161], which makes it possible to assess the adequacy of the model based on the probability of observing the output data using a concrete model. Friston et al. [162, 163] present a detailed description of the procedures for the choice of models and selection of parameters.

2.4.2 Granger causality. In addition to the methods for determining effective connections based on a neuronal interaction model, there is a family of approaches using observational experimental data alone. The most popular of them is the Granger causality test [164]. In its classical form, Granger causality is a linear mathematical apparatus for the statistical testing of the hypothesis of whether the information about process X is of value for predicting process Y based on two principles: (1) the cause precedes the effect; (2) the cause has unique information about the future meanings of the effect.

The null hypothesis for testing Granger causality is formulated as follows:

$$P\left(Y(t+1)|I(t)\right) \neq P\left(Y(t+1)|I_{-X}(t)\right), \tag{34}$$

where $Y(t+1)$ is the next value of process $Y(t)$ to be predicted, and $I(t)$ and $I_{-X}(t)$ are complete information and information excluding process X, respectively, available by the time point t. According to the Granger causality principle, process X is the cause of process Y provided that the null hypothesis (34) is accepted.

In the multidimensional case, the Granger causality analysis is performed as a fitting of the vector autoregressive

model to the available time series. Let $X(t) = \{X_1(t), X_2(t), \ldots, X_D(t)\}$ be a multidimensional (multichannel) time series of dimension D; then, Granger causality is expressed in the form

$$X(t) = \sum_{l=1}^{L} A(l)X(t - l\Delta t) + \varepsilon(t)\,, \tag{35}$$

where L is the time delay, Δt is the time series sampling step, and $A(l)$ is the matrix of regression coefficients for each value of the delay l. The time delay L is determined in accordance with the Akaike criterion [165] or the Schwarz criterion [166]. Based on expression (35), the time series X_i predicts the time series X_j if at least one element of $A_{i,j}(l)$ $(l = 1, \ldots, L)$ differs significantly from zero.

The Granger causality analysis has a number of important limitations. First, it is sensitive to the common input problem and can yield ambiguous results in the form of false connections in the case of more than two time series. Second, the results of the causality analysis may be incorrect in the case of nonlinear nonstationary time series. Third, in the traditional formulation, the method is aimed at identifying linear patterns and cannot reveal nonlinear interactions. Modifications of the method for the analysis of nonlinear connections have been proposed in a number of papers [167–169].

The Granger causality analysis was adapted for use in the frequency domain [170–172], which is important for the analysis of experimental neurophysiological signals. Estimates of directed interactions between brain regions in the frequency domain can be obtained using multivariate autoregressive models [173]. After fitting the multivariate autoregressive model to signals at the sensor level or at the source level, directed interactions can be quantitatively determined using a directed transfer function [174] or partial directed coherence [171, 175].

Note also that Granger causality in the source space was carried out by a number of research teams [93, 94, 103, 176, 177]. Astolfi et al. [93, 94] applied structural equation modeling in addition to the directed transfer function to evaluate effective connections using both simulated and recorded high-resolution EEG data. These approaches were further modified to enable the calculation of time-varying effective connections using adaptive multivariate autoregressive models [178].

3. Integration processes in the brain

The human brain interacting with the environment is incessantly involved in cognitive processes associated with the treatment of sensory information and its analysis, decision-making, and control of motor functions. Under real conditions, the cognitive processes are inextricably linked to one another, in contrast to those under conditions of a special neurophysiological experiment designed so as to be focused on the effects associated with one of the processes and to neutralize the influence of others. In the context of neural activity, these processes correspond to integrative dynamics of the cerebral cortex characterized by functional interaction among its different parts.

The important role of functional interactions in the cortical neuronal network during realization of cognitive and behavioral functions is confirmed by neuroimaging data [179–182]. Specifically, the results of fMRI indicate that the brain realizes its functions through the interaction among various functional subnets, both in the passive waking state and under a cognitive load. By now, a large number of functional subnets have been discovered, viz. the 'dorsal network of attention support,' 'fronto-parietal network,' 'executive control network,' and 'network of the passive mode of brain operation' [183]. These subnets are located in different parts of the cerebral cortex, but they interact with one another during cognitive activity, the efficiency of which depends on the degree of functional integration of cerebral neuronal networks [184].

Results of research show that mental fatigue leading to a decline in cognitive abilities is accompanied by a decrease in the effectiveness of interactions between different subnets [185]. It also confirms the need for functional integration to support an effective cognitive activity. Finally, the activity of the brain under cognitive load conditions is also associated with an increase in the degree of integration within the cortical network to ensure access to additional resources. According to [186], an enhanced cognitive load lowers modularity in the functional brain network. In this case, the network of the passive mode of brain operation strengthens connections with other subnets, while its own internal connections weaken.

It can be concluded that the integrative dynamics of the distributed cortical network of the brain mediated through the functional interaction among its various parts support sensory-motor and cognitive activity; they also permit dynamically managing cognitive resources to maintain the high efficiency of brain work.

Let us consider a number of important examples of integrative processes in the functional networks of the brain associated with the treatment of sensory information, the planning of motor acts, and pathological activity during epilepsy. To begin with, here is a brief introduction to the mathematical apparatus of the graph theory used to describe characteristics of reconstructed cerebral functional networks [31, 187] (see Section 3.1).

3.1 Mathematical apparatus of the theory of complex networks

3.1.1 Basic definitions. From the mathematical point of view, the functional network of the brain can be represented as a graph [2, 36, 188]. An undirected (directed) graph $G = (\mathcal{N}, \mathcal{L})$ contains a set of nodes (or vertices) $\mathcal{N} \equiv \{n_1, n_2, \ldots, n_N\} \neq 0$ and many unordered (ordered) pairs of nodes $\mathcal{L} \equiv \{l_1, l_2, \ldots, l_K\}$ which represent the edges (or connections) of the graph [189]. If the number of elements in $\mathcal{N}$ and $\mathcal{L}$ corresponds to the number of network nodes N and the number of links K, a graph defining the network can be denoted as

$$G_{N,K} = (\mathcal{N}, \mathcal{L})\,. \tag{36}$$

A network node is usually described by the number i in the set $\mathcal{N}$. In an undirected graph, each connection is determined by a pair of nodes, i and j, and is denoted (i, j) or l_{ij}. Two nodes connected by an edge are called adjacent or neighboring. In a directed graph, the order of the two nodes is important: l_{ij} denotes the link directed from the ith node to the jth one, while $l_{ij} \neq l_{ji}$. The usual way to graphically represent a graph is to draw a point for each node and connect the two points with a line if the two corresponding nodes are connected. How these points and lines are drawn is of no consequence: the only thing that matters is which pairs

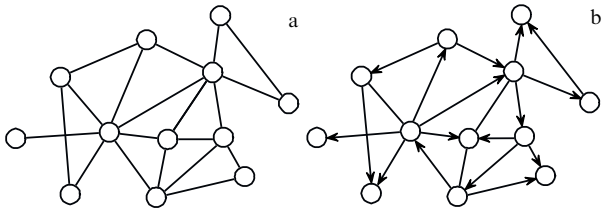

Figure 7. Examples of undirected (a) and directed (b) graphs with $N = 12$ and $K = 18$.

of nodes form a connection and which do not. Examples of undirected and directed graphs with $N = 12$ and $K = 18$ are presented in Figs 7a and b, respectively. For a graph of size N, the number of edges lies within $0 \leqslant K \leqslant K_N = N(N-1)/2$. Graph G is called sparse if $K \ll N^2$ and dense if $K = O(N^2)$. A graph is termed complete if $K = K_N$, i.e., when all nodes are connected to each other.

Moreover, the notion of a weighted graph is introduced:

$$G_{N,K}^{W} = (\mathscr{N}, \mathscr{L}, \mathscr{W}), \tag{37}$$

which includes, in addition to numerous nodes $\mathscr{N}$ and links $\mathscr{L}$, a set of quantities usually referred to as weights, $\mathscr{W} \equiv \{w_1, w_2, \ldots, w_K\}$, which are the real numbers associated with the connections $\{l_1, l_2, \ldots, l_K\}$. In this case, two nodes are characterized not only by the presence of a connection between them but also by the weight (intensity) of the connection (interaction).

The central concept in graph theory is the reachability of two different nodes in a graph. In fact, two nodes that are not adjacent may nevertheless be 'available' to move from one to the other. A transition from node i to node j is an alternating sequence of nodes and edges (a sequence of neighboring nodes) that starts with i and ends with j. The length of the path from the ith node to the jth one is defined as the number of edges in this sequence. A path between two nodes is a transition in which no node is visited more than once. The minimal distance between two nodes is usually called the shortest path. In addition, the concept of a closed path is introduced; it consists of at least three nodes of a cycle in which no edge is repeated. A cycle of length k is usually called the k-cycle, denoted by C_k. C_3 is the simplest cycle, referred to as a triangle. A graph is called connected if for each pair of different nodes i and j there is a path from the ith node to the jth one; otherwise, the graph is considered disconnected.

In the network theory, it is convenient to consider the matrix representation of a graph. The graph $G_{N,K}$ (36) can be fully described by specifying the adjacency (or connectivity) matrix A, i.e., a square matrix $N \times N$ whose element a_{ij} ($i, j = 1, \ldots, N$) equals 1 when link l_{ij} exists and 0 if otherwise. In other words, the adjacency matrix is symmetric for undirected graphs and contains $2K$ nonzero elements. The weighted graph $G_{N,K}^{W}$ (37) is represented as a square matrix of weights W $N \times N$, elements of which, w_{ij}, are equal to the weight (intensity) of the connection between the ith and jth nodes; $w_{ij} = 0$ for unconnected nodes.

In the graph theory, various characteristics of graphs are distinguished, which can be conditionally divided into two groups: (1) segregation measures reflecting the possibility of identifying some subnets within the network (clustering and modularity of the network); (2) network integration measures describing certain aspects of the effectiveness of communication among all nodes inside the analyzed network.

3.1.2 Network integration and segregation. Studies on human and animal brain networks in the context of the theory of graphs have demonstrated a nonrandom organization of functional cerebral connections, including the tendency of nodes (i.e., brain regions) to cluster into organized ensembles [1]. The tendency of the brain toward local clustering is combined with a high throughput of information flows, as evidenced by the high efficiency and the small average path length of functional brain networks formed, for example, while processing sensory information [2, 190, 191]. A combination of the high degree of global integration of the brain network with the presence of hub nodes showing high centrality and enhanced efficiency of local information processing suggests the presence of such a type of network organization of the brain as small world topology [192].

A graph of the 'small world' type has the following property: two arbitrary vertices i and j are not adjacent with a high probability, but one is reachable from the other by a small number of transitions through other vertices. The typical distance L between two arbitrarily chosen vertices i and j, defined as the number of steps needed to reach one from the other, increases in proportion to the logarithm of the number of vertices N in the network: $L \propto \log N$. This type of network architecture promotes local information processing and at the same time allows information to be effectively integrated throughout the system [193].

In Refs [1, 194, 195], a hypothesis was put forward that suggests that the modular structure of the neural network is beneficial for the brain, since high connectivity between the elements in one module contributes to the local (in terms of the entire network) realization of specialized functions, e.g., primary processing of sensory information [195], while reducing the cost of organization of the information flow between different areas of the brain [196].

It should be noted that a number of experimental studies [197–199] have produced evidence of a high degree of coincidence between the functional and structural modules of the central nervous system in health and disease. Specifically, it has been shown that the modular structure of the brain's functional network and the associated structure of cerebral functional subsystems are interconnected via a relatively small number of densely connected brain nodes with high centrality (hubs) [200, 201] confined to the frontal and parietal regions of the cortex and the central lobe of the brain [202]. It has been shown that the totality of white matter tracts connecting these nodes of the brain's functional network with a high degree of centrality at relatively large distances consists of large axonal projections [203–205].

In fact, the connections between the hubs of the functional brain network topologically form a 'central highway' for the global 'neuronal traffic' in the brain. This core of connected hubs forms a system called the 'rich club' [201]. Importantly, such a system is not free from drawbacks, despite the advantages due to the high efficiency of information transfer within a similarly organized network. Suffice it to say that lesions in the connections between the 'rich club' nodes disrupt information transfer in the system as a whole [206], which may seriously interfere with the performance of motor acts after a stroke and result in the physical destruction of part of the neuronal ensemble of the brain [207, 208].

Network integration measures reflect the efficiency of communication among all nodes in the entire network. The simplest characteristic describing the number and density of connections in the network is the degree k_i of the ith node, which can be defined in terms of the adjacency matrix as

$$k_i = \sum_{j \in \mathcal{N}} a_{ij} . \tag{38}$$

If a graph is directed, the degree of the node consists of two components: $k_i = k_i^{\text{out}} + k_i^{\text{inp}}$, where $k_i^{\text{out}} = \sum_j a_{ij}$ is the number of outgoing connections and $k_i^{\text{inp}} = \sum_j a_{ji}$ is the number of incoming connections.

The basic topological characteristic of a graph G can be obtained in terms of the distribution of degrees $P(k)$ of the nodes, defined as the probability that a node chosen at random has the degree k or as the fraction of nodes in the graph having the degree k, which is equivalent. Information about how the degrees are distributed between the nodes can be obtained either by constructing $P(k)$ or by calculating the moments of distribution:

$$\langle k^n \rangle = \sum_k k^n P(k) . \tag{39}$$

The first moment $\langle k \rangle$ is the average degree of a network node and is often used in the analysis of real networks.

The shortest paths in the network play an important role in internode communication. If, for example, some data need to be sent from one node to another, the paths of a minimum length are optimal for the fastest transfer and saving resources. For this reason, the shortest paths, like the degrees of nodes, play an important role in the internal structure of the network. It is convenient to represent all the lengths of the shortest paths of graph G in the form of matrix D, where the element d_{ij} is the minimal length of the path from node i to node j. Based on matrix D, it is possible to introduce an important characteristic describing the integration of network nodes, i.e., the length of the shortest path averaged over all pairs of nodes:

$$L = \frac{1}{N(N-1)} \sum_{i,j \in \mathcal{N}, i \neq j} d_{ij} . \tag{40}$$

The connection of two nonadjacent nodes, say j and k, depends on the nodes belonging to the paths connecting these nodes. Therefore, a measure of 'importance' of a given node in the network can be obtained by counting the number of shortest paths passing through it and determining the so-called intermediate centrality of the node. Along with the degree of a node, intermediate centrality is one of the standard node centrality measures in the network. The strictly intermediate centrality b_i of the ith node is defined as

$$b_i = \sum_{j,k \in \mathcal{N}, j \neq k} \frac{n_{jk}(i)}{n_{jk}} , \tag{41}$$

where n_{jk} is the number of shortest paths connecting the jth and the kth nodes, and $n_{jk}(i)$ is the number of shortest paths connecting the jth and kth nodes and passing through the ith node.

Turning back to the topology of complex networks, one can distinguish between homogeneous and heterogeneous networks. The homogeneity of a network structure implies that almost all its nodes are topologically equivalent, as in regular lattices or random graphs. In the latter, for example, each of the $N(N-1)/2$ possible connections is present with an equal probability, which means that the distribution of node degrees is either binomial or Poisson-type in the large graph size limit. Homogeneous networks in the brain are exemplified by 'small world' networks describing the features of cerebral functional networks of a subject at rest [209].

Heterogeneous networks are characterized by a highly nonuniform distribution of the degrees of nodes determined by the presence of hub nodes connected with many other ones. The hubs are often present together with a large number of weakly connected elements. A typical example of such networks is provided by freely scalable networks characterized by a power-series distribution in the form of the power law $P(k) \sim k^{-\alpha}$ with exponents $\alpha \in (2, 3)$. Thus, hubs are nodes with a high degree of centrality, as shown in Fig. 8a. Their presence is a marker of the structural ordering and hierarchical organization of a complex network.

The main marker of the structural ordering in the brain, regarded as an integrated complex network system, is the deviation of the distribution of node degrees $P(k)$ in a functional network from the Poisson distribution. Studies of functional brain networks have demonstrated the distribution of the degrees of nodes with 'heavy tails' [210–212], which suggests the existence of a number of highly connected areas [213]. Certain areas of the brain are characterized by a higher degree, low clustering, short path length, and high centrality. They are actually hubs in the functional network of the brain [200, 214]. Such hubs play a central role in establishing and maintaining effective communication among brain regions, which is critically important for its normal functioning [215, 216].

To recall, high-centrality nodes tend to bind more tightly to other hubs than do low-centrality ones. As is mentioned above, this integration phenomenon is referred to in terms of the network theory as the 'club of the rich' by analogy with social systems in which well-connected high-centrality individuals not infrequently tend to unite in clubs [217, 218] (Fig. 8b). The presence or absence of a 'club of the rich' can yield important information about the network structure, especially about its stability, hierarchical ordering, and specialization [218, 219]. For example, a strong tendency toward integration of power grids into 'rich club'-like systems arises from the necessity to create grids capable of readily distributing electricity from one station to another to reduce the likelihood of a critical failure. On the other hand, the absence of 'club of the rich' structures in protein interaction networks reflects the high level of their functional specialization. References [201, 220–222] report examples of the tendency to organize cerebral functional networks into structures with 'rich club' properties.

An analysis of integration in the brain's networks requires an understanding of segregation in a functional network and knowledge of its internal structure. The most typical situation of network segregation is the formation of a structure called the community structure. Such organization means that the nodes of a network can be easily combined into groups (communities or modules) characterized by a high density of connections between those nodes belonging to a given group and sparser connections between the communities. However, there are situations in which communities may overlap. Therefore, in the general case, to define a network as a structure of communities, it is necessary to establish the fact that pairs of nodes are more likely to be connected if they are both members of the same community and less likely to be

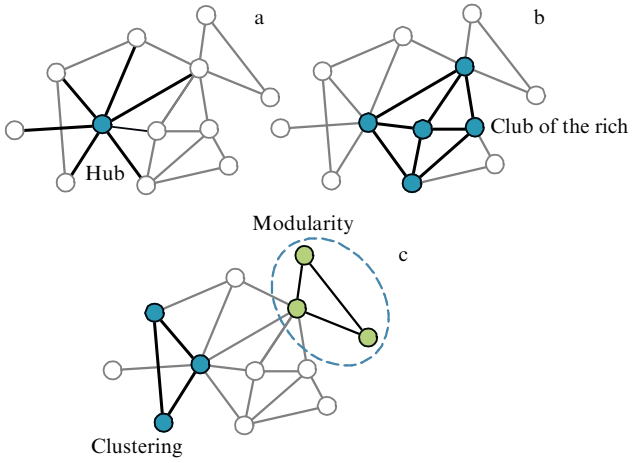

Figure 8. (Color online.) Examples of integration in complex-topology networks: (a) a node with high centrality (hub), (b) a rich club-like structure, and (c) examples of segregation of the formation of dedicated structures (a cluster and a module).

such if they belong to different communities. Elucidation of the structure of communities in complex networks is a powerful tool for understanding the structure and function of a network and mechanisms of its restructuring.

There are a large number of methods making it possible to analyze segregation in the cerebral network, with special emphasis on its communities and the degree of clustering. Their general goal is to find meaningful divisions into groups by analyzing the structural properties of the entire graph and introducing certain network segregation measures to characterize the degree to which the network can be split into local structures (clusters or modules) with a large number of inter-element connections inside them. At the same time, such structures have a small number of connections that link them to the rest of the network, as shown in Fig. 8c presenting examples of the formation of dedicated structures in the network.

The simplest and at the same time the most common effect of segregation in a network is clustering, also known as transitivity, which suggests a connectivity structure in which two nodes communicate with each other with a greater probability if they are linked to the third one [31]. Another example of segregation in a network is the modularity effect, reflecting the fact that the network as a whole can be divided into separate modules or communities with a high density of internal connections contrasting with the low density of connections between a module and the rest of the network.

To analyze modularity, the algorithm of Girvan and Newman [223] is widely used for breaking a network into components in an iterative process based on the identification and gradual removal of connections with the largest distances. Because the edges of a graph lying between communities are expected to have the greatest length, their recursive removal may ensure an acceptable division of the network into communities. A number of modifications and additions to this algorithm have been proposed for the search for modularity in complex cerebral networks [224–226], including structural and functional ones [227–229].

Structural and functional networks of the brains of humans and higher animals are characterized by a high degree of clustering and modularity, which may serve as one of the criteria for the detection of pathological conditions of the brain. For example, there is a tendency towards a reduction in clustering of structural connections in the connectome of patients with schizophrenia compared to that in control subjects [230]. The effect of impaired clustering is especially well pronounced in the frontal, temporal, parietal, and cerebellar regions of the brain [231], which confirms the general tendency to clustering impairment in the connectome of patients presenting with schizophrenia. Results of the studies of the cerebral functional network in schizophrenics suggest, in general, reduced clustering [232, 233]. Examination of such patients using fMRI have revealed simultaneous impairment of clustering and modularity in brain functional networks in cases of schizophrenia developed in childhood [234].

3.1.3 Multilayer functional networks of the brain. It should be noted that the traditional models of cerebral networks in the form of graphs described in the preceding paragraphs illustrate only one way of interaction between network nodes. At the same time, such neuroimaging technologies as fMRI, MEG, and EEG record the dynamics of brain regions in time in different frequency ranges. It is often important to store and compare information about the spectrum dynamics in different frequency ranges [235–239]. For example, the perception of a visual stimulus is accompanied by a decrease in the amplitude in the alpha range (8–12 Hz) and its increase in the beta range (20–30 Hz) in the occipital region of the brain [240]. In addition to the measurement of functional interactions using fMRI/fNIRS or MEG/EEG, methods for the *in vivo* elucidation of the connectome structure, such as diffusion tensor imaging (DTI) [241], detect the presence and measure the strength of physical connections between different brain regions.The availability of multimodal datasets requires a quantitative model universal and flexible enough to describe interactions among different scales and modalities in order to obtain a deeper insight into the brain's organization.

To solve this problem, it was proposed to use multilayer networks to simulate many complex interactions in brain functional networks [242–244]. A multilayer network is a generalization of a traditional network making possible a network description of multimodal data [245, 246]. Multilayer networks are built on the basis of a weighted graph (37) of a traditional network with the addition of a supplementary set of layer indices $s\colon \mathscr{N} \to \mathscr{S}$ — from a set of nodes to a set of layer indices $\mathscr{S}$, i.e.,

$$M^{W}_{N,K,D} = (\mathscr{N}, \mathscr{L}, \mathscr{W}, \mathscr{S})\,. \tag{42}$$

It is assumed that the set of layer indices has the form $\mathscr{S} = S_1 \times S_2 \times \ldots \times S_D$, where each set $\mathscr{S}_i$ is called the ith layer of a multilayer network, and the network itself in this case is D-dimensional. From the point of view of the graph theory, the only difference between traditional and multilayer networks is that, in a traditional network, each node is assigned a label $n_i \in N$, whereas, in a multilayer network, a vector label $\mathbf{s}(n_i) = (n_i^1, n_i^2, \ldots, n_i^D)$ is assigned to each node. In the multilayer formalism, it is possible, in essence, to construct several levels of traditional networks, with each level describing some feature or aspect of multimodal data. Intralayer connections serve the same purpose as in a traditional network; they reflect connections between nodes

on a layer representing a single property of the modeled data. Interlayer connections provide a description of interaction among various properties of a single node. This permits considering several modes of interaction between the nodes of a multilayer network characterized by a vector of properties.

Let $S_1 = H$ be the number of nodes on each layer which are physical objects (e.g., a sensor on the head surface during EEG/ MEG). Let us denote the nodes of the network by the index i ($i = 1, \ldots, H$) and the number of nodes in the total network by the index v ($v = 1, \ldots, N$, $N = DH$). Figure 9a illustrates the difference between the nodes and vertices in a multilayer network.

Multilayer networks can also be described in terms of matrix formalism, like traditional networks. For each pair of vertices in a network with indices i and j, it is possible to introduce weight w_{ij} corresponding to the connection between these vertices. One can also introduce the supra-adjacency matrix $\bar{A}$ for a multilayer network $M^{W}_{N,K,D}$, analogous to the adjacency matrix of a traditional network, i.e., a square matrix $DH \times DH$ in size with elements $a_{ij} = w_{ij}$ that can be represented as the block matrix

$$\bar{A} = \left(\begin{array}{c|c|c|c} A^1 & E^{12} & \ldots & E^{1D} \\ \hline E^{21} & A^2 & \ldots & E^{2D} \\ \hline \vdots & \vdots & \ddots & \vdots \\ \hline E^{D1} & E^{D2} & \ldots & A^D \end{array}\right), \qquad (43)$$

where matrix blocks A_i are the adjacency matrices for vertices on the ith layer, and E^{kl} are the matrices containing the weights of connections between the vertices of the kth and lth layers of the network. For the model network presented in Fig. 9a, Fig. 9c shows the structure of its matrix, where the dark cells correspond to intralayer connections, gray cells, to interlayer connections, and white cells, to the absence of connections.

There are various approaches to the reconstruction of connections in multilayer networks in relation to modeling brain networks. One of them is to take into account fMRI, EEG/MEG (functional connections) and DTI (structural connections) data for an individual person, which makes it possible to build a multilayer network with two layers of functional and structural connections (see, for example, [247], where fMRI data were used to construct a two-layer network).

fMRI or EEG/MEG data can be used to build a functional network, with the nodes representing brain regions and connections reflecting the statistical relationship between activities in each region. Taking account of the DTI data allows a structural network to be constructed by dividing the brain into regions again and measuring the strength of the connections between them. Finally, a multilayer brain network is constructed by adjusting each of these functional and structural networks to the corresponding layers of the multilayer network (Fig. 10a). Another example is the reconstruction of multilayer functional networks based on multichannel temporal fMRI, MEG, or EEG data. This method consists of decomposing a signal into several frequency bands for each brain region and subsequently assessing the functional similarity between the regions in each of these frequency ranges after the reconstruction of the respective layers. Figure 10b shows an example with two layers corresponding to two frequency ranges, α (8–12 Hz) and β (20–30 Hz). Interlayer connections can be added in a variety of ways [248], e.g., by connecting all brain regions to

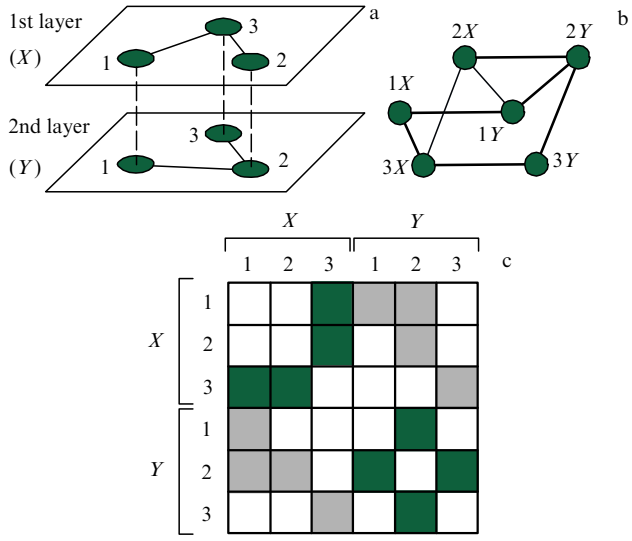

Figure 9. Different representations of a multilayer (two-layer, for simplicity) network. Representation of the network in the form of a graph with reference to network division into layers (a), where intralayer connections are shown by solid lines and interlayer connections, by dashed lines. Classical representation of a network graph (b) with identical connections (shown by solid lines). (c) Adjacency matrix, the same for both representations. Intralayer connections in the matrix are marked with a dark color, the interlayer connections are gray, and the absence of bonds is white.

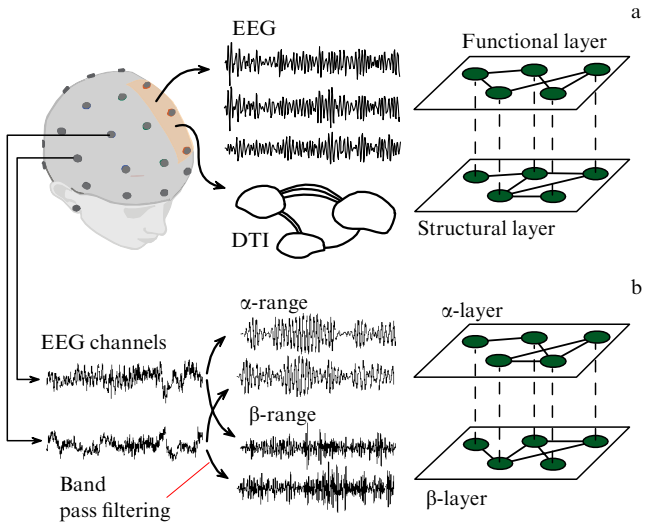

Figure 10. Illustration of the construction of a multilayer functional network of the brain according to neuroimaging data. (a) Accounting and comparison of EEG (the layer of functional connections) and DTI (the layer of structural connections) data, (b) network layers corresponding to functional connections in different frequency ranges.

themselves through all layers [239, 249] or by measuring the similarity of signals between the layers [250, 251].

Multilayer networks of the brain provide a powerful analytical tool; the most difficult aspect of their construction appears to be the reconstruction of connections between vertices on different layers corresponding to a single network node. This procedure is difficult to formalize and the question remains open from the standpoint of a correct mathematical procedure. One of the simplest methods is to use a multiplex network model [252] assuming all interlayer connections to be

similar and having weight w_0. In this case, the super-adjacency matrix (43) contains the matrix blocks $E^{kl} = w_0 I$, where I is the identity matrix of dimension H.

3.2 Functional networks formed during processing of visual sensory information

The perception and processing of sensory information are the main functions of the brain that ensure the interaction of a living organism with the environment. Life processes are associated with the continuous receipt of sensory information (tactile, visual, auditory, etc.), its processing, and further use for making decisions. It is known that certain parts of the cerebral cortex are involved in the processing of various types of sensory information. For example, visual information is processed in the occipital and parietal cortex, while auditory information is treated in the temporal lobes.

However, the spatial differentiation of the above processes occurs only at the stage of primary processing, i.e., within the first tens of milliseconds after the presentation of the stimulus. At subsequent stages, sensory processing is an integration process that combines the analysis of various types of sensory information and the identification of characteristic features of sensory data required for decision making. In this case, neuronal ensembles of the prefrontal and parietal cortex associated with attention and working memory are activated, in addition to the areas responsible for primary sensory processing. Along with the integrative dynamics of the neural network of the cerebral cortex caused by simultaneously proceeding cognitive processes, the processing of sensory information can also involve additional areas of the cerebral cortex when the magnitude and complexity of the processed stimuli increase.

Let us consider the integration processes taking place in the neural network of the cerebral cortex in association with processing visual information. To begin with, it should be noted that sensory processing in the brain is carried out under the influence of two processes: top-down and bottom-up, each involving different neuronal populations and activating different functional connections between them. The ascending processes are associated with involuntary attention activated by visual stimuli [253]; they control information processing in the primary visual cortex at the early stages of perception. The descending processes are, in turn, associated with conscious stimulus processing. One such process is selective attention, which determines the ability of a subject to distinguish characteristic features of sensory information necessary to make a decision [254, 255]. The descending processes are formed in the cerebral cortex and affect the processes of perception and processing of visual information in deeper structures.

Thus, a visual stimulus activates an ascending process which triggers its processing in the primary visual cortex. This process begins in the visual zone V1 located in the occipital lobe of the cerebral cortex. The visual area V1 transmits visual information along two visual pathways: dorsal and ventral, as shown in Fig. 11a.

The dorsal path begins in the primary visual zone (V1), passes through visual zone V2, then goes toward visual zone MT (also called V5) and to the posterior part of the parietal lobe of the cerebral cortex. The dorsal path is associated with motion, the idea of object location in space, control of eye movements, and the use of visual information for assessing the reachability of objects. The ventral pathway also begins in the V1 zone and passes through V2, but then goes through

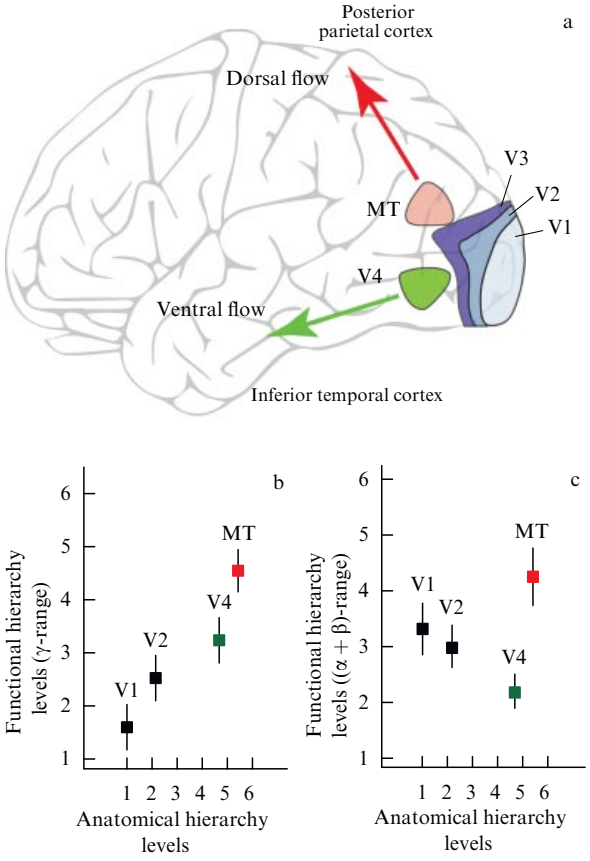

Figure 11. (Color online.) (a) Two paths of the ascending visual information processing flow. The lower part of the figure shows connections between the anatomical hierarchy of the regions of the cerebral visual cortex and the functional hierarchy deduced from the directionality of connections calculated for high-frequency γ (b) and low-frequency (α + β) (c) ranges using MEG signals. (Based on data from [256, 257].)

visual zone V4 toward the ventral (lower) part of the temporal lobe of the cerebral cortex. The ventral pathway operates in the processes of shape recognition, the formation of the idea of an object, and the functioning of long-term memory. Interaction between different visual areas occurs through anticipatory and feedback neuronal connections. The presence of anticipatory and feedback loops is determined by the hierarchical structure of the visual cortex [256]. The anticipatory connections are directed from primary zone V1 to the higher-level zones within the ventral and dorsal pathways. Feedback, in turn, is oriented opposite to the direction of the visual pathways, its final target being the V1 zone [257].

In primary visual perception, the transmission of information within the ventral and dorsal pathways is carried out through functional neuronal connections. An analysis of neural activity recorded invasively in different parts of the visual cortex of primates demonstrates the leading role of low-frequency α-rhythms (8–12 Hz) and β-rhythms (15–30 Hz), as well as high-frequency γ-rhythms (> 50 Hz) in neuronal interaction involving both anticipatory and feedback connections [256]. Invasive recording in humans, in contrast to that in primates, is problematic, but a comparative analysis of invasive recordings in monkeys and noninvasive recordings in humans indicates a similar hierarchy of visual cortex regions [258]. In addition, it has been shown that, in humans, as in monkeys, the low-frequency (α + β (8–30 Hz)) and high-frequency (γ) neuronal activities ensure the trans-

mission of information along feedback and anticipatory connections, respectively.

To elucidate the functional hierarchy, the authors of [258] applied a method for reconstructing directed connections based on Granger causality with the use of magnetoencephalography data. For each pair of regions, the strength and directionality of communication in the low-frequency $(\alpha + \beta)$- and high-frequency γ-ranges were determined. Based on the coefficients obtained for each area, the directed influence asymmetry index (DIAI) was calculated (Fig. 11b, c). Large DIAI values indicate a high position of the area in the functional hierarchy where neurons experience a stronger impact from the lower levels. It was shown that the functional hierarchy calculated on the basis of connections in the γ-range coincides with the anatomical hierarchy (Fig. 11b). This means that upstream information is propagated through high-frequency neuronal interactions.

An analysis of the hierarchy of functional neuronal connections in the $(\alpha + \beta)$-range revealed an inverse correlation with the anatomical hierarchy in the case of ventral flow (Fig. 11c). This result suggests that the downstream transmission of information is mediated through neuronal interactions in the low-frequency $(\alpha + \beta)$-range. To conclude, visual zones V4 and MT belonging to high levels of the anatomical hierarchy of the ventral and dorsal streams occupy different positions in the functional hierarchy based on the analysis of interactions in the $(\alpha + \beta)$- and γ-ranges. The authors of [258] attribute this to peculiarities of the processed visual information.

The role of functional neuronal connections involved in the downward flow of visual information processing is considered in Refs [259, 260]. The authors of Ref. [259], in contrast to those of [258], calculated connections separately in the α- and β-frequency ranges using the wavelet bicoherence method. The authors of [259] considered the connections among five regions of the occipital-parietal cortex by analyzing EEG signals recorded from the head surface at the sensor level. It was shown that the perception of a visual stimulus is accompanied by the strengthening of functional connections in the neural network of the occipital-parietal cortex in the α- and β-frequency ranges.

The characteristic structure of connections is illustrated by Fig. 12a, where the line thickness reflects their strength. It can be seen that, in the frequency ranges considered, the strengthening of the connections takes place both within the occipital and parietal regions and between them. The influence of the complexity of visual information on the structure of functional connections was also considered. Figure 12b shows connections that strengthen with increasing complexity of sensory information. It can be seen that the increased complexity promotes the strengthening of the connections inside the parietal region in the β-range and of the connections between the parietal and occipital regions within both ranges.

Summarizing the results of the above work, it can be supposed that, although the interaction within the descending flow occurs in the α- and β-frequency ranges, the interaction in the β-range is most pronounced in the parietal region as the complexity of the processed information grows. This assumption is consistent with the hypothesis of the existence of a center of attention in the parietal cortex functioning due to neuronal interactions in the β-frequency range [261].

Attention is known to be one the main descending processes that control the perception and processing of

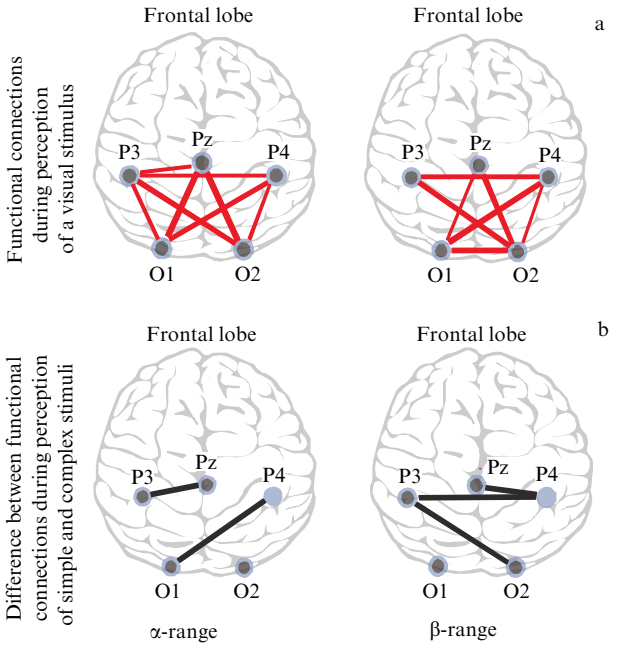

Figure 12. (a) Functional connections reconstructed by the analysis of wavelet bicoherence in α- and β-frequency ranges during perception of a visual stimulus. (b) Functional connections in α- and β-frequency ranges strengthening with growing complexity of the visual stimulus. (Based on data from [259].)

sensory information. This process involves neuronal populations of the frontal and prefrontal cortex, besides those of the parietal region, thus forming a distributed fronto-parietal cortical network. Functional interactions among the neuronal populations in the fronto-parietal cortical network are possible owing to the synchronization of neural activities among brain regions in the β-range.

It is known that the involvement of various parts of the fronto-parietal network is associated with an increase in the volume and complexity of the information being processed. A small amount of sensory information can be easily processed within the parietal region. An increase in the amount of information to be processed requires additional resources provided by the involvement of the frontal and prefrontal cortex [262], as confirmed by an analysis of experimental data. However, the mechanisms underlying the formation of functional connections between distant neuronal ensembles are still hypothetical. Reference [135] considers coherent resonance induced by an external influence in the cortical neural network to be one of the possible mechanisms behind such functional interaction.

Coherent resonance is a well-known phenomenon in the theory of nonlinear oscillations, involving the fact that the response of an auto-vibrating system to an external influence becomes most coherent in the presence of an optimal noise level at the excitation boundary [263–265]. When an excitable system is the network of a large number of elements, coherent resonance is such that most of them exhibit synchronous activity in response to an external influence in the presence of internal noise [266–268]. The authors of [135] hypothesize, by analogy with a network of self-oscillating elements and a cortical neural network, that the formation of coherent neural activity under the influence of internal noise should also demonstrate the effect of coherent resonance. The presence of noise in the neuronal ensemble of the brain is well known.

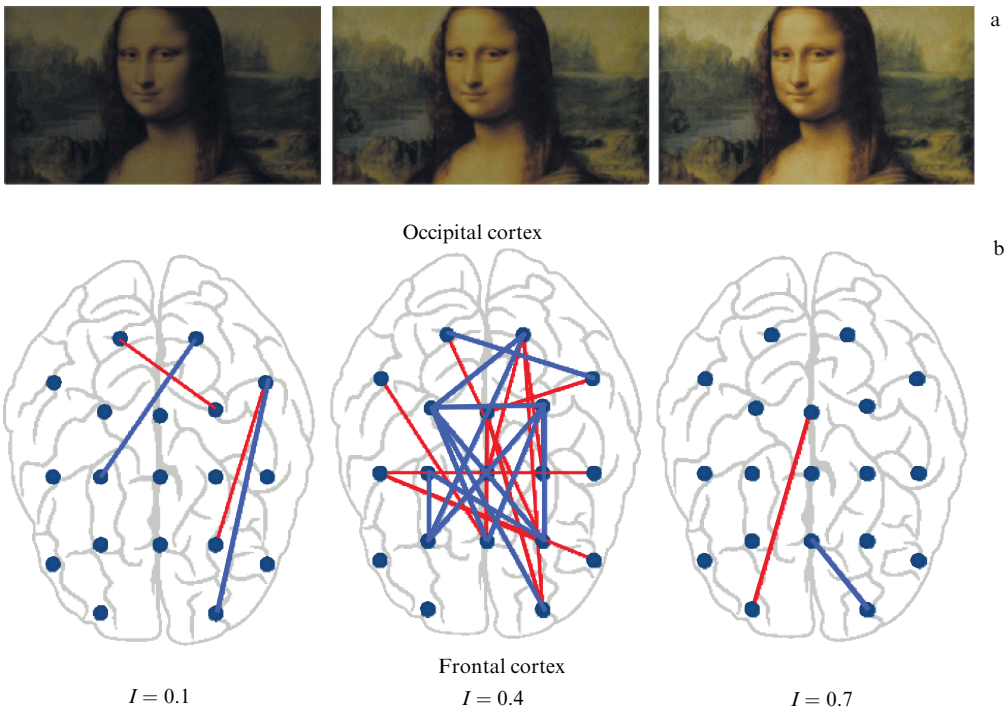

Figure 13. (Color online.) (a) Three visual stimuli (Mona Lisa by Leonardo da Vinci) differing in contrast intensity *I*. (b) The structure of functional connections in α- and β-ranges (red and blue lines, respectively) corresponding to the processing of visual stimuli with different contrasts. (Based on data from [135].)

The sources of noise are, in particular, fluctuations caused by the opening and closing of ion channels [269–271].

To detect coherent resonance in the neural network of the brain, experiments were carried out to register EEG signals in subjects undergoing visual stimulation. Copies of Leonardo da Vinci's Mona Lisa differing in contrast intensity were shown several times to each of them. Examples of images with three levels of contrast are presented in Fig. 13a.

It is known that an enhancement of image contrast increases the frequency of neuron generation in deep brain structures involved in the primary processing of visual information [272]. These neurons then excite the cortical network, in which further processing takes place. An analysis of experimental data shows that the greatest coherence of the neural activity in the cerebral cortex is observed at a certain intermediate level of image contrast. The experimental results obtained indicate that the behavior of the neural network of the brain demonstrates the coherent resonance effect. The effect is observed at different contrast intensities in different people because characteristics of internal noise are individual for each subject (see, for instance, [273]).

It is worthy of note that the activation of neuronal populations in the frontal cortex and the strengthening of functional connections coordinating the activities of these two areas are observed when an optimal-contrast image is presented. Fig. 13b shows the structure of functional connections in the α- and β-frequency ranges for different contrast versions of the images. Evidently, a distributed fronto-parietal functional network is formed at an intermediate contrast level, meaning that internal noise in the brain's neural network improves the effectiveness of processing a visual stimulus by virtue of coherent resonance that, in turn, coordinates integration processes in large neuronal ensembles.

As discussed above, the reconfiguration of the structure of functional connections and the involvement of additional regions of the cerebral cortex are due to both the varying complexity of sensory information and the integration of sensory processing into other cognitive processes, such as decision making. The use of machine learning methods in [274] to investigate visual information processing under uncertainty conditions showed that decision-making in the case of a high degree of uncertainty takes about 0.6–0.8 s, while the classification of unambiguous stimuli requires much less time (0.3–0.4 s). According to [16, 275], the stages of sensory processing and decision-making can be separated both in time and in space. For example, processing a visual stimulus occurs within the first 0.2 s after its presentation and is characterized by synchronization of neural activities in the occipital and parietal regions. The decision-making process begins at subsequent stages and is characterized by the involvement of the frontal and prefrontal cortex with the establishment of strong functional connections between them.

From the standpoint of the formation and reconfiguration of functional neuronal connections, this process is discussed at length in [16], where the brain activity in a group of human subjects was analyzed during the perception and interpretation of a bistable image, a Necker cube. The subjects had to press a button corresponding to one of two interpretations of the bistable stimulus within a short time interval of 1–1.5 s. To reconstruct functional connections, changes in the EEG signal energy in the α- and β-frequency ranges were calculated from the results of a continuous wavelet analysis. The functional connections were then reconstructed from the values obtained using the recurrent interaction measure [276]. Variations in the intensity of connections between brain regions were compared with its level in the pre-stimulus period of the EEG. Two adjacency

matrices, M_{inc} and M_{dec}, containing connections with increasing and decreasing weights, were introduced. In this case, the reconfiguration of the functional network is described by the ratio of the numbers of the strengthening and weakening connections:

$$R = \frac{\sum_{i=1}^{N}\sum_{j=1}^{N} M_{\text{inc}}(i,j)}{\sum_{i=1}^{N}\sum_{j=1}^{N} M_{\text{dec}}(i,j)}, \qquad (44)$$

where N is the number of EEG channels.

An analysis of the structure of functional connections revealed a number of features related to decision-making. It was found that 0.3 s before pressing the button, the test subjects experienced a strengthening of the neuronal connections in the β-range described by an increase in the proportion of functional connections R (44) strengthened during perception of a visual stimulus (Fig. 14a). A detailed analysis of the network structure was carried out by calculating the degrees of nodes for outgoing connections $k_{i,\text{inc}}^{\text{out}}$ (38) using the adjacency matrix M_{inc}. The $k_{i,\text{inc}}^{\text{out}}$ value was shown to increase during the time period that preceded making a decision (Fig. 14b), while the greatest value of the degrees of nodes was recorded in the frontal cortex. An analysis of the structure of functional connections showed that the increase was associated with both a rise in the density of connections inside the frontal cortex and a greater number of outgoing connections directed towards the occipital region (Fig. 14b, time point t_3). The results obtained confirm the theory that high-level processes associated with the treatment of sensory information, its interpretation, and subsequent decision-making are realized through the activation of the fronto-parietal functional network. It is shown that the leading role in this network is played by the frontal regions.

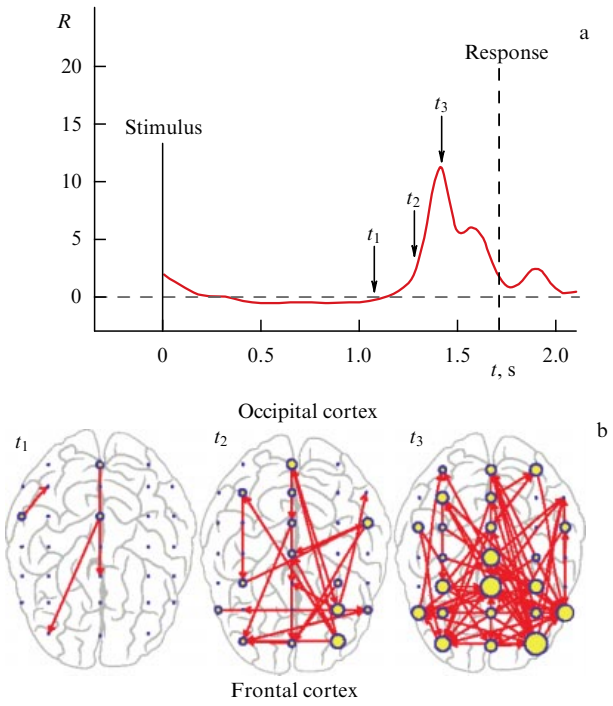

Figure 14. (Color online.) (a) Proportion of functional connections R (44) strengthening upon perception of a visual stimulus. The vertical dashed line corresponds to the response of the test subject (pressing the button). (b) The structure of functional connections at characteristic time points $t_{1,2,3}$ of functional network reconfiguration. The size of the node in the network characterizes its degree $k_{i,\text{inc}}^{\text{out}}$ in terms of outgoing connections. (Based on data from [16].)

The main result of Ref. [16] is the establishment of the fact that the structural characteristics of functional connections do not depend on the complexity of a visual stimulus. This means that a brain processing sensory information selects a set of characteristic features of the stimulus necessary for making a decision [277]. It can be assumed that the pre-decision processes associated with the extraction of the relevant characteristics of the stimulus depend on its complexity and take longer time as the complexity increases.

It can be concluded that the processing of sensory information is an integrative process that combines interacting ascending processes at the initial stages of stimulus perception and interacting descending processes associated with an increase in the cognitive load (complexity of information) and the enhanced relationship between sensory processing and other processes, such as decision-making. The ascending processes are associated with the formation of functional neuronal connections in the high-frequency γ-range and the descending ones, with the formation of connections in the lower-frequency β-range.

3.3 Integration and segregation of the functional brain network in planning motor activity

The motor functions of the human brain, together with its cognitive activity, are naturally exploited in everyday life. These two forms of brain work are closely inter-related, which is easy to explain in terms of the development of bipedalism (a form of terrestrial locomotion where an organism moves by means of its two rear limbs or legs). This type of motion with the body in an upright position enables human beings to resist gravitational effects, keep balance, and control the mode of their gait. Taken together, these actions led to the necessity of processing a large amount of sensory information and converting it into motor commands. It is assumed that it was the evolution of human bipedal locomotion that led to a genetic mutation which, in turn, initiated the formation of large neuronal populations responsible for the execution of logical purposeful movements followed by the development of cognitive functions and consciousness [278, 279].

There are a number of publications in support of this hypothesis. Specifically, it is known that motor and cognitive processes take place in one spatial-frequency domain of neural activity of the brain. Namely, low-frequency α/μ- and β-rhythms are observed in the frontal and sensorimotor regions of the cerebral cortex, where their interaction ensures the planning of various actions and control over their implementation. Moreover, it was shown that the development of attention promotes successful motor activity [280], and episodic memory is involved in motor control in animals [281]. Also, a number of studies demonstrated that cognitive activity develops more intensively when there is an urgent need to perform more complex motor functions [278, 282].

It should be specially emphasized that cognitive and motor functions of the brain develop in close connection with each other over the entire lifespan of a human; they determine the mechanisms of structural and functional reorganization of the brain at various stages of its development [278]. For example, the postural activity needed to maintain a certain position of the body in space, explore the surrounding world, and learn empirically may be reduced in childhood. This slows down the development of the cerebral cortex and cerebellum and thereby causes a disruption of the

coordination among neural activity rhythms underlying the relationship of cognitive and motor activities. Therefore, developmental disorders, as well as confusion of the brain integrative dynamics, equally affect normal cognitive and motor functions [283].

From the point of view of normal brain functioning, the overlapping areas of the cortical neural network responsible for the performance of cognitive and motor functions become excited when someone watches the movements of outsiders and at the stage of planning one's own movements. In the first case, the interaction between the motor and cognitive functions implies the involvement of long-term memory and the extraction of information relevant for understanding and interpreting actions of the surrounding people. In the second case, this interaction guarantees accurate planning and precise implementation of the planned actions. In such situations, the phase of planning a movement is inextricably linked with the subsequent execution of the motor act, because human movements are not simple reflexes evoked by external commands or stimuli. As a rule, they are planned and performed to achieve a certain goal. Therefore, a motion is a result of a series of complex cognitive processes taking place at all stages, from the formulation of a motor task and its planning to the performance and control of motor functions. Obviously, the solution to such a complicated problem stimulates the interaction and integration of several parts of the brain, ensuring the execution of various functions [279].

Motor processes in the brain are supported by several centers of motor control located in the motor cortex (Fig. 15a). The central part of the motor cortex of the brain is the primary motor cortex (M1). Its main task is low-level control of well-developed motor activity; the neuronal ensemble of this area directly controls the work of the muscles. In addition to control in the primary motor cortex, control over minor and more specific motor activities, as well as over sequential movements, is performed in the premotor cortex (PMC). The supplementary motor area (SMA) supports planning movements. In this regard, the integrative dynamics of the motor cortex obeys a functional hierarchy at the base of which is the Ml cortex for processing information about movements of the basic type, then comes the PMC ensuring the performance of more complex motor functions, and last, at the upper level of the hierarchy, is the SMA, responsible for high-level processing of information related to planning and controlling targeted actions. This description emphasizes the functional segregation of motor cortex regions of the brain with reference not only to the importance of the functions they perform but also to the interaction among them that ensures the successful execution of deliberate actions.

Figure 15b illustrates the effective connections between regions of the motor cortex reconstructed by dynamic causal modeling (DCM) [159, 286]) as applied to fMRI data [284] in a group of healthy subjects asked to clench their right hands into a fist. It can be seen that a movement of the right hand enhances connectivity in the opposite left (L) part of the motor cortex with simultaneous suppression of the activity in M1 and SMA of the right (R) hemisphere.

An analysis of the number of strengthening outgoing connections shows that the neural processes associated with the free execution of movements are controlled by the supplementary motor cortex of the corresponding hemisphere and transmit commands to the primary and premotor regions. These regions receive sensory information from the muscles and receptors through a feedback mechanism; they also exchange information with each other and thereby ensure successful control of movements.

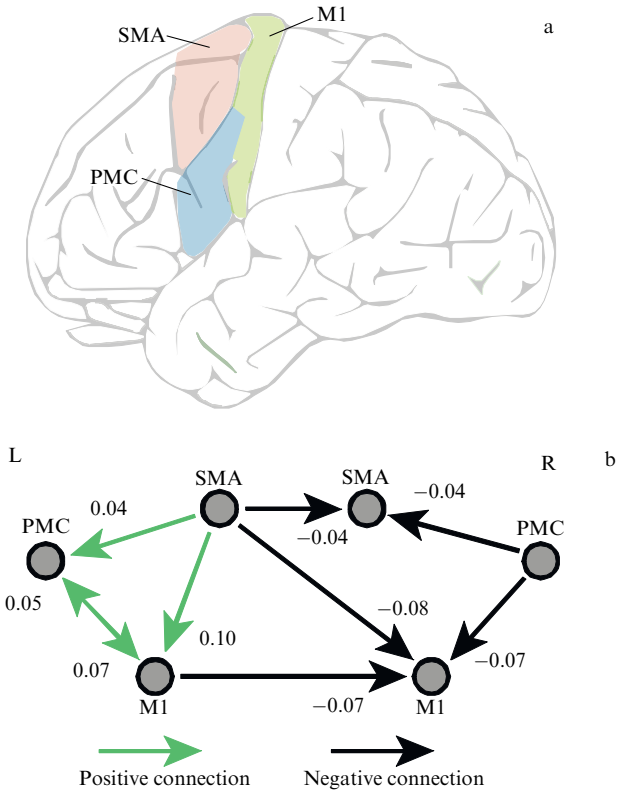

Figure 15. (Color online.) (a) Parts of the human cerebral motor cortex: primary motor cortex (MI), premotor cortex (PMC), supplementary motor area (SMA). (b) Functional connectivity between parts of the cerebral motor cortex during right hand movement in a control group of healthy participants in FMRI studies. (Based on data from [284].)

The relationship between cognitive and motor functions of the human brain is also confirmed by the ability to imagine motor activity. Imagining movements is a specific cognitive task consisting of mental representation of a motor act without its subsequent execution. There are two types of imaginary motor activity: kinesthetic and visual. The former is imagining or planning limb movements 'in the first person'; the latter is imagining the execution of movements watched from the sidelines [287]. It is kinesthetic imaginary motor activity that activates overlapping regions of the cerebral cortex involved in the actual performance of movements, whereas visual imaginary activity has a quite different structure associated largely with the prefrontal cortex [288]. Moreover, imaginary and real motor activities differ significantly in terms of connectivity of the cerebral motor cortex.

A comparative analysis of effective connections in the motor cortex identified on the basis of the Granger causality was undertaken in the framework of fMRI studies using the grapho-theoretical approach [285]. The significant differences in the topology of the effective connections in the motor cortex were found to be associated with real and imaginary movements of the right and left hands (Fig. 16). Indeed, since an imaginary movement precedes a real one, its execution naturally strengthens principal connections and activates additional ones. Moreover, a closed circuit is excited between the primary motor (M1) and primary somatosensory (S1) regions in the hemispheres opposite to

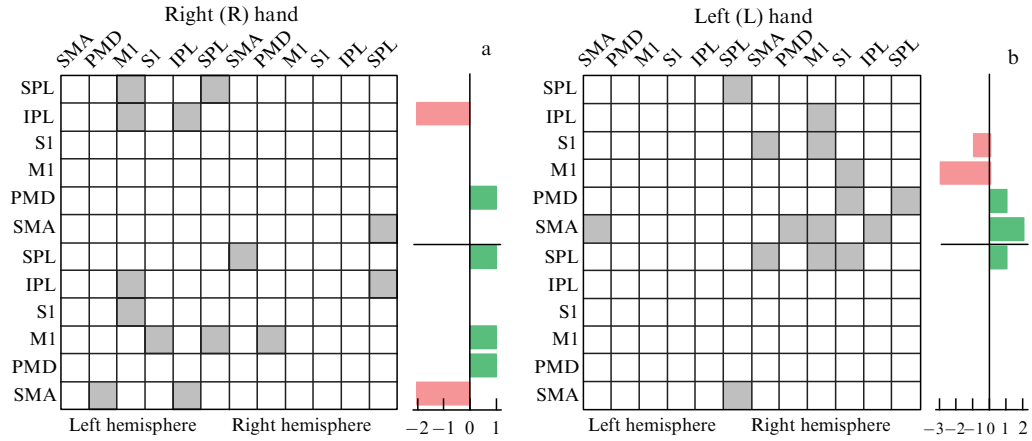

Figure 16. (Color online.) Strengthening effective connections in the cerebral motor cortex during real movement compared with effective connections during imaginary right (a) and left (b) hand movements of the same type ($p < 0.05$, paired Student's test with Bonferroni correction). For each connection matrix, a histogram of the difference between incoming and outgoing connections is presented on the right side (modified from [285]).

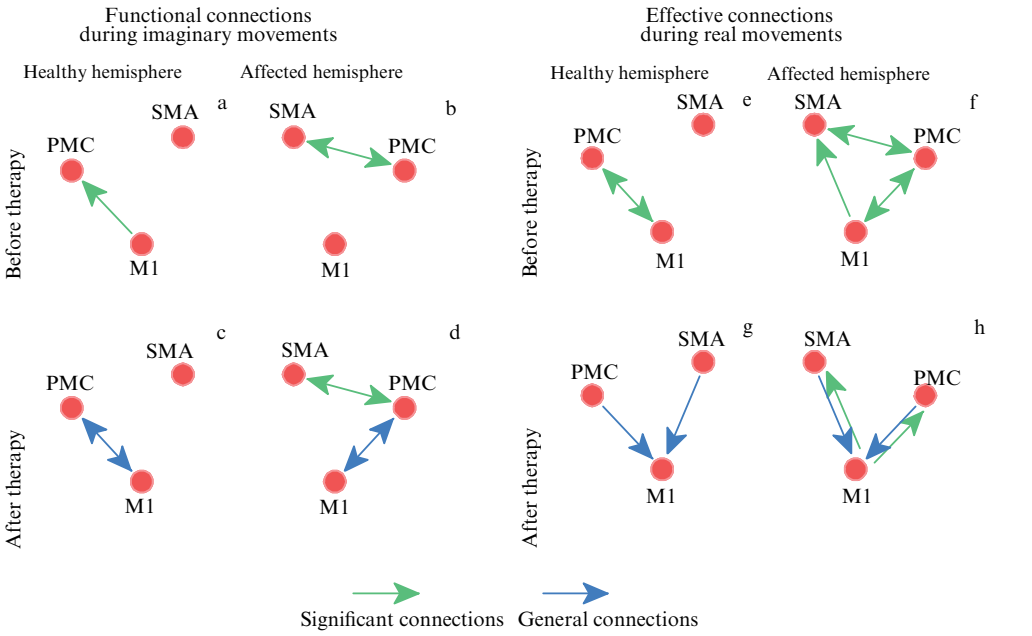

Figure 17. (Color online.) Reconfiguration of functional connections in the motor cortex during imaginary (a–d) and real (e–h) movements before (a, b, e, f) and after (c, d, g, h) therapy in healthy (a, c, e, g) and affected (b, d, f, h) hemispheres. Meaningful connections were selected based on the $p < 0.05$ criterion using Student's statistical test. (Based on data from [298].)

the type of movement performed (right or left hand). It is known that S1 supports the individual experience of sensing one's own body [289], while M1 is involved in the processing of sensory information needed to perform a forthcoming action [290]. The strengthening of integration between the somatosensory and motor functional networks suggests that the brain turns not only to the processing of external sensory information but also to its own earlier experience to successfully perform motor acts, which makes it possible to effectively develop and train more accurate motor functions.

The described interactions among different parts of the brain in healthy people undergo significant changes in patients who have suffered a stroke that caused significant changes in the structure of neuronal connections in the motor cortex due to damage or death of the nerve tracts linking its various regions [291, 292]. This, in turn, seriously impairs motor functions and lowers the general cognitive background in post-stroke patients.

A number of studies have addressed mechanisms of reorganization of functional connections in the motor cortex from the perspective of developing strategies for the rehabilitation of the lost functions and restoration of normal brain operations [293, 294]. One of the effective methods for training motor functions is mental practice, including imagining motor activity, since it activates the same parts of the motor cortex and the connections between them that are involved in the execution of real motor actions [295, 296]. Furthermore, a positive effect in the form of the strengthening of functional connections between the premotor and primary motor cortex was demonstrated in post-stroke patients as a result of rehabilitation procedures including mental practice and physical therapy [292, 297].

Reference [298] demonstrates mechanisms of reorganization of functional connections among different parts of the cerebral motor cortex in stroke patients that promote the improvement of motor functions under the effect of therapy.

Figure 17 illustrates the related changes in the functional connections between parts of the motor cortex. The formation of symmetric connections at the level of reconfiguration of the motor cortex functional network in the healthy and affected hemispheres was observed during performance of similar tasks in the post-treatment period. Imagining movements gave rise to a closed circuit between the premotor and primary motor cortex common to both hemispheres (Fig. 17c, d). The execution of real movements resulted in connections between the additional motor and primary motor cortex common to both hemispheres, as well as between the premotor and primary motor cortex (Fig. 17g, h). At the same time, the behavioral characteristics of the performed movements calculated using Fugl–Meyer indices [299] improved after therapy; they positively correlated with the strength of the effective connection between the premotor and accessory motor cortex ($r = 0.94$), as well as between the primary and premotor cortex ($r = 0.87$).

Thus, the execution of motor activity is a consequence of interaction among several parts of the cerebral motor cortex. Moreover, these parts show a strict functional hierarchy, which ensures their activation and interaction at different stages of the fulfillment of motor tasks for planning and controlling movements. Many studies show that a disturbance of such interactions worsens the quality of movement performance in patients with severe neurological symptoms.

3.4 Functional interaction between brain regions before and during an epileptic seizure

One of the most well-known types of brain activity characterized by the functional interaction between different cerebral regions is associated with an epileptic seizure. An electroencephalographic marker of this pathological activity is a peak-wave discharge, i.e., high-amplitude oscillations with a well-pronounced fundamental frequency. Such activity in the cortex and deep-lying structures of the brain is recorded in several EEG channels at a time. For example, this activity in the somatosensory cortex and thalamic nuclei of rats with absence epilepsy contributes to the formation of a functional thalamo-cortical network responsible for the onset and development of an epileptic attack [300, 301]. To recall, absence epilepsy is characterized by nonconvulsive (non-motor) seizures (absences).

Figure 18 presents recordings of electrical activity in a rat brain at the onset of an episode of absence epilepsy (the beginning of the seizure is denoted by the vertical dashed line). The recordings were obtained with the use of high-impedance invasive electrodes implanted into the somatosensory cortex (S1) and thalamic nucleus (Po) [302]. Figure 18a shows signals characterizing the activity of individual neurons recorded using spike sorting algorithms. Figure 18b illustrates the total activity of large neuronal ensembles in the cortex and thalamus. It can be seen that the onset of an attack corresponds to a high- amplitude rhythmic activity. Oscillations of the total electric potential have the form of sharp surges (spikes) followed by a low-frequency oscillation (wave). A comparison of Figs 18a and b gives evidence that spike generation frequencies in the cortex and thalamus coincide; moreover, a similar frequency is recorded in the signals of activity of individual neurons.

It can be argued that an epileptic seizure is a global synchronization mode involving neurons located in different parts of the cerebral cortex and thalamic nuclei and synchronizing the activities of these regions. In other words,

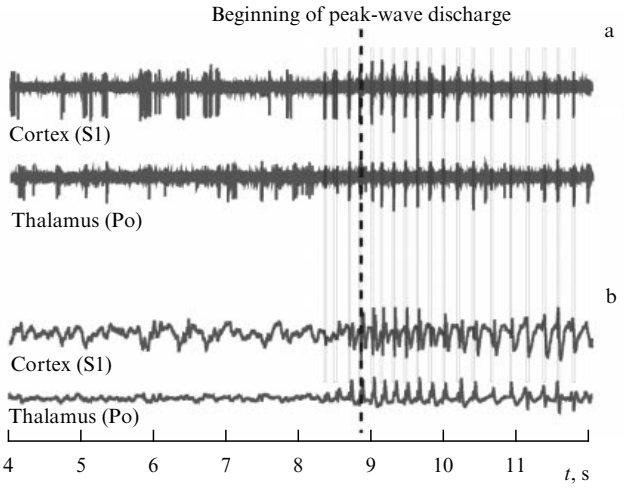

Figure 18. Recordings of electrical activity in the rat brain at the onset of a peak-wave discharge: (a) the activity of individual neurons and (b) the total activity of neuronal ensembles in the cortex S1 and thalamus Po. (Based on data from [302].)

the epileptic activity is associated with the formation of a characteristic structure of functional connections. The detection of the peculiar patterns inherent in this process can, on the one hand, contribute to understanding the factors responsible for the development of an attack and, on the other hand, enable prediction of an attack and even its prevention, e.g., by the destruction of functional connections [301]. To reconstruct them, various methods are used based on the time-frequency analysis of nonlinear associations and causality, recurrent analysis, and artificial intelligence methods.

Let us consider the application of various methods for the reconstruction of functional connections, e.g., the analysis of the thalamo-cortical network in the brain of WAG/Rij rats genetically predisposed to absence epilepsy. WAG/Rij rats are a valuable model for *in vivo* studies of epilepsy [303]. Animals with advanced epilepsy are known to experience several ten seizures per hour, which makes it possible to collect good statistics for testing algorithms [304]. According to the results of neurophysiological studies, the thalamo-cortical network plays a key role in the formation of an epileptic seizure.

Consider a set of signals of neural activity recorded using seven chronically implanted electrodes in: (1) layers 4–6 of the somatosensory cortex; (2) the posterior thalamic nucleus (Po); (3) the ventral postero-medial thalamic nucleus, VPM); (4) the anterior thalamic nucleus, ATN); and (5) the reticular thalamic nucleus (RTN). Based on the fact that an epileptic seizure is characterized by synchronous oscillations in a frequency range of 5–10 Hz [305], it seems appropriate to focus on the reconstruction of functional connections in this region of the spectrum.

In Ref. [302], this process was realized in two ways, viz. by the traditional method for calculating wavelet bicoherence and using a technique based on the degree of similarity between vibration spectra. The latter approach permits determining the degree of coherence between u_{ij} signals based on the relation

$$u_{ij} = \left[\int_{f_1}^{f_2} \left| W_i(f) - W_j(f) \right| \mathrm{d}f \right]^{-1}, \qquad (45)$$

where f_1 and f_2 are the boundaries of the frequency range being considered and $W_{i,j}(f)$ are the amplitudes of the wavelet spectra of the analyzed EEG signals. In Ref. [302], a continuous wavelet transform with a Morlet wavelet frequently applied to process neurophysiological data was used [306]. Normalized values $W_{i,j}(f) = \Delta f\, W_{i,j}(f) / \int_{\Delta f} W_{i,j}(f')\, df'$ were taken for the calculation. To obtain the normalized values, the spectral amplitude calculated for the $[f_1, f_2]$ range was divided by the energy of the spectrum calculated for a wider range Δf. Due to this, $W_{i,j}(f)$ reflected the part of the spectral energy concentrated in the frequency range of interest. In [302], a rise in $W_{i,j}(f)$ was associated, first, with the fact that most of the neuronal ensemble was involved in rhythm generation at frequencies $[f_1, f_2]$ and, second, phase coherence of activity in this group of neurons increased.

It follows from the above that large values of coefficient (45) indicate that neuronal populations of a comparable size in the neuronal ensembles i and j participate in generating activity in the $[f_1, f_2]$ range. In contrast to wavelet bicoherence, the method under consideration disregards phase relationships among the analyzed signals. This simplification makes it possible to reduce the time needed to calculate a correlation among several channels, which allows the use of a real-time approach in the seizure prediction interface [301, 307].

Figure 19a shows coherence coefficients of electrical activity signals from the brain calculated in a 5–10 Hz frequency range using wavelet bicoherence (w) and the degree of coherence (u) (45). The coefficients are averaged for the signals recorded in the cerebral cortex and thalamus. First, it can be seen that the values calculated on the basis of the two approaches are in excellent agreement with each other. Second, the characteristic features of the cerebral cortex and thalamus associated with the onset of an epileptic seizure can be identified. It appears that the neural activity of the cortex is characterized by a rise in coherence within a few seconds after the onset of an attack. In the thalamus, coherence reaches a maximum during the first 5 seconds after the onset of the seizure and thereafter decreases. A comparison of the signals of electrical activity recorded in the cortex and thalamus at the onset of an attack (t_1) and 10 s after (t_2) shows that synchronization increases between cortical channels and decreases between thalamic channels (Fig. 19b).

These results suggest that the onset of an epileptic seizure is associated with an enhancement of functional interaction between the neuronal populations of the cerebral cortex and thalamus leading to the synchronization of oscillations of the electric potential in a frequency range of 5–10 Hz. During an attack, the interaction between the neuronal ensembles of the cerebral cortex increases, while it decreases between the thalamic populations

In a recent study [117], the functional interaction between neuronal populations of the thalamo-cortical network was determined based on the assessment of generalized synchronization (see Section 2.3.4). Generalized synchronization of two dynamic systems implies a functional relationship between their states. To elucidate this functional dependence, a machine learning technique was used in the form of an artificial neural network (ANN). It was shown that 3 s before the onset of an attack (Fig. 20a) the connections between neuronal populations were present in both the cerebral cortex and the thalamus. This means that the onset

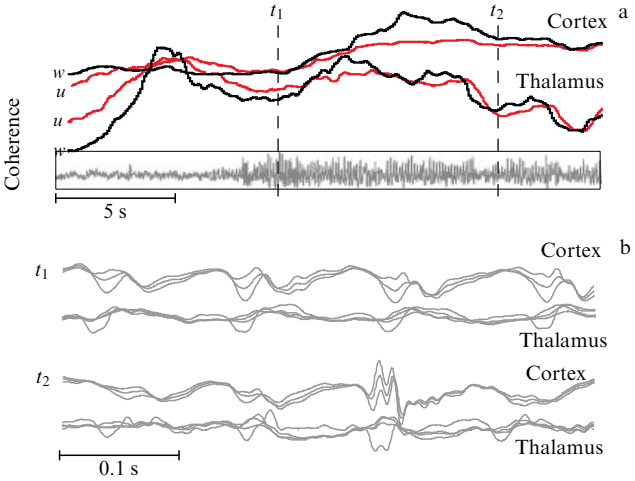

Figure 19. (Color online.) (a) Correlation coefficient of electrical activity in the cerebral cortex and thalamus calculated using wavelet bicoherence (w) and based on the similarity of the spectra (u). (b) Oscillations of the electric potential registered in cortical and thalamic channels at the onset of an attack (t_1) and 10 s after (t_2). (Based on data from [302].)

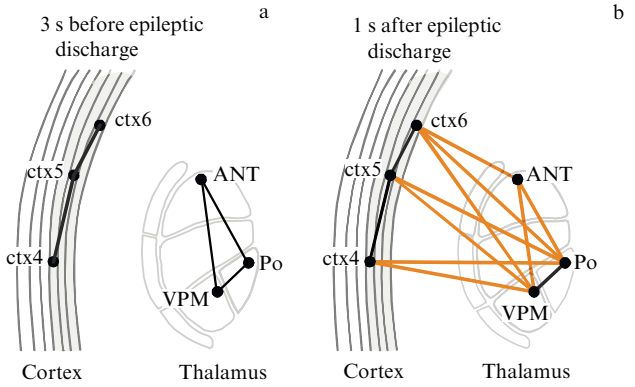

Figure 20. Functional connections in the thalamo-cortical network reconstructed using machine learning (ANN) methods 3 s before (a) and 1 s after (b) the onset of an epileptic seizure. (Based on data from [117].)

of an epileptic seizure is accompanied by the establishment of a functional connection between the cortical and thalamic neuronal populations (Fig. 20b).

The above observations suggest the necessity of strengthening functional connections between neuronal populations of the cerebral cortex and thalamus for the development of an epileptic seizure. Strengthening connections promotes a functional relationship between variations of the electrical potential recorded in these brain areas. A time-frequency analysis shows that the establishment of the functional connection synchronizes activities of these areas in a frequency range of 5–10 Hz, which corresponds to epileptic activity. Synchronization of the activity in the cortex and thalamus takes place at the onset of an attack and is accompanied by the strengthening of functional connections in both the cortex and the thalamus, as well as between them (Fig. 20b). During the attack, the signals in the thalamus undergo desynchronization, while synchronization persists in the cortex. It can be supposed that in this case the cortex supports the formation of the epileptic seizure, whereas the weakening of functional connections between the cortex and the thalamus gradually leads to a loss of epileptic activity in

thalamic neuronal populations, which results in the termination of the discharge.

Observations reported in preceding paragraphs suggest the leading role of the cerebral cortex in the development of an epileptic seizure and the need for a functional interaction between the cortex and the thalamus for its generation. However, which brain region, the cortex or the thalamus, initiates the attack remains to be clarified. Identification of the part of the brain responsible for the onset of an epileptic seizure is of primary importance in the context of clinical research. It is necessary not only to assess the degree of interaction (strength of connection) but also to determine which area of the brain affects others (i.e., to determine the direction of connections).

In Ref. [308], this problem was addressed using the Granger causality method (see Section 2.4). The authors documented the strengthening of connections between neuronal populations of the cerebral cortex 2 s before the onset of a seizure. One or two seconds prior to the attack, the connections directed from the cortex to the thalamic nuclei Po, ANT, VPM, and RTN formed. Simultaneously, feedback outgoing from the thalamic nuclei Po, ANT, and VPM toward cortical neuronal populations ctx4, 5, 6 appeared. The data obtained indicate the leading role of cortical neuronal populations in the initiation of an epileptic seizure. These findings are confirmed by the results of the reconstruction of the connections using the previously described recurrent interaction measure.

Figure 21 shows the directed connections undergoing significant strengthening 2 s (Fig. 21a) and 1 s (Fig. 21b) before the onset of the seizure. The big red dot indicates the node with the largest number of outgoing connections. The key role of the cerebral cortex (layers 5 and 6) is well apparent during the time period preceding the discharge. Two seconds prior to the attack, the cortical connections and the connections between the cortex and the thalamus become strengthened. The connections outgoing from layer 5 of the cerebral cortex (ctx5) to thalamic nuclei ANT and Po appear. The records obtained from the RTN thalamic nucleus are not considered in the case under discussion, but Ref. [308] gives evidence of the strengthening of connections between RTN and other thalamic nuclei (Po, ANT, and VPM). It can be assumed that the interaction between neuronal ensembles of the cortex and thalamic nuclei is mediated through the thalamic nucleus RTN, in agreement with Ref. [308].

Strengthening connectivity between cortical regions 5, 6 and the thalamic nucleus Po is confirmed in [309] by the nonlinear association method (see Section 2.3.2). These data also suggest the leading role of the cerebral cortex in the development of an epileptic attack, and the relationship between the cortical regions and the thalamic nucleus Po is considered to be an indispensable condition for the induction of a seizure. The leading role of Po in the generation of the attack has been demonstrated in [310]. A phase consistency analysis [311] shows that the onset of the seizure is associated with the strengthening of connectivity between Po and the remaining thalamic nuclei.

A time-frequency analysis of preictal activity [310] reveals an increase in the spectral energy in the somatosensory cortex. According to the results described in preceding paragraphs, a rise in the spectral energy of a neuronal ensemble can be due either to the involvement of a larger part of the ensemble or to the establishment of phase synchronization between the activities of individual neurons. The preictal activity is

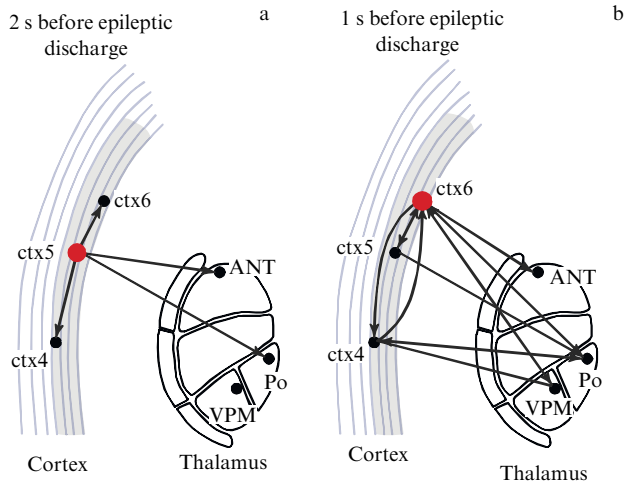

Figure 21. (Color online.) Directed functional connections in the thalamo-cortical network reconstructed using the recurrent interaction measure in the preictal period 2 s (a) and 1 s (b) before the onset of epileptic discharge.

characterized by phase synchronization in the neuronal ensembles of the cortex and the thalamus, leading to an increase in the spectral energy of recorded electrocorticographic signals within a certain frequency range. Because an epileptic seizure is associated with the interaction of the cortex and the thalamus, it can be supposed that the spectrum of signals recorded in both these regions during the preictal period is characterized by a simultaneous increase in the energy in a certain range.

It was shown in [312] that the onset of an epileptic attack is preceded by the formation of time-frequency patterns of 'discharge precursors' in the cortex and thalamus characterized by a local increase in the energy in the frequency ranges θ/α (5–11 Hz) and δ (3–5 Hz) simultaneously in both areas of the brain. Thus, the precursors, along with the peak-wave discharge itself, are also characterized by synchronization of the neural activity in the thalamo-cortical network of the brain. An analysis of a large number of seizures in a group of experimental animals showed that 80–90% of the attacks were accompanied by the appearance of θ/α- and δ-precursors of the epileptic discharge simultaneously in the cortex and thalamus.

To sum up the results of this section, it can be concluded that the onset of an attack of absence epilepsy is accompanied by the strengthening of functional connections among neuronal populations of the thalamo-cortical network. A large number of studies show that the key role in the development of an attack is played by the cortical neuronal populations that affect the thalamic structures. Results of the reconstruction of functional connections by various methods indicate that the connections among cortical neuronal populations become strengthened 2 s before an attack; thereafter, cortico-thalamo-cortical connections begin to appear. On the contrary, the destruction of the discharge is associated with the disintegration of the thalamo-cortical connections and the release of thalamic nuclei from the formed functional brain network.

4. Network brain–computer interfaces

Brain–computer interfaces (BCIs) are devices for interaction between humans and the environment by means of reading

and decoding signals of brain activity and translating them into control commands for external devices [313]. The principle of operation of traditional BCIs is schematically illustrated in Fig. 22. As a rule, BCIs distinguish meaningful signs based on the analysis of neural activity recorded separately by each sensor (univariate data analysis [314]).

Over recent decades, BCIs have been successfully used not only to control external devices but also to control and restore the sensorimotor functions of the human brain [315, 316]. The greatest successes have been achieved in the sphere of motor BCIs used to rehabilitate impaired human motor functions or to control devices by generating imaginary motor commands by the BCI operator [317, 318]. First and foremost, this is due to the fact that the relationship between motor activity and the underlying neural activity of the brain has been fairly well studied and represents readily reproducible and stable patterns characterizing a human being [319–321], which allows accurately tuning algorithms for decoding motor commands. Second, input parameters for motor BCIs may be signals from both single neurons and a collection of neurons in the case of invasive recording, as well as signals of the electrical activity characterizing the total electric field of local neuronal groups (noninvasive EEG). At the same time, invasive methods of recording neural activity provide an opportunity for an accurate classification of more complex movements [322], while EEG is a more convenient technology for addressing everyday and rehabilitation tasks [323, 324].

At the same time, a number of studies show significant inter-subject variations of sensorimotor activity patterns [325, 326]. They are manifested as the variability of frequency ranges of the characteristic neural activity rhythms, the magnitude of the spectral power of excited or suppressed oscillations, and the location of the sought patterns in space. As a result, the accuracy of real-time recognition of imaginary activity patterns usually does not exceed 70–80%. As follows from the materials presented in Sections 2 and 3, the functional connections forming between cerebral cortex regions may serve as more relevant and stable signs of ongoing cognitive and motor processes. Thus, the network properties of brain functioning can also be employed as basic elements of new-type BCIs, so-called network BCIs, (Fig. 22). The latter differ from traditional ones in that they analyze fundamentally multichannel data in order to form a vector of signs based on information about functional relationships between brain areas.

A recent review [66] reports successful examples of network BCIs that use functional connections in the brain as reference signs for deciphering neural activity associated with the imagination of movements. In particular, the authors of [327] use a network metric based on the phase synchronization of EEG signals to assess the structure of the emerging network of functional connections during the movement of the fingers on the right and left hands. Hidden Markov networks were used to evaluate and classify the resulting network structures. The proposed method proved more efficient than the traditional assessment of evoked desynchronization of the μ-rhythm in the motor cortex in a group of 15 subjects.

The authors of [328] investigated the efficiency of network BCIs for the recognition of imaginary movements of arms and legs using the metrics derived from the vector autoregressive models to assess effective connections. It was shown that the use of the direct transfer function to assess the effective connections ensures an acceptable accuracy of the movement classification in the framework of traditional approaches to the estimation of the μ-rhythm spectral power in the motor cortex. Interestingly, other methods considered in Ref. [328] demonstrate a significantly lower accuracy.

The reconstruction of functional networks based on phase synchronization has also been successfully applied for the classification of imaginary hand movements in [329]. The authors compared the functional relationships calculated from the value of the α-rhythm phase capture using a multichannel EEG signal filtered in the 6–14-Hz frequency

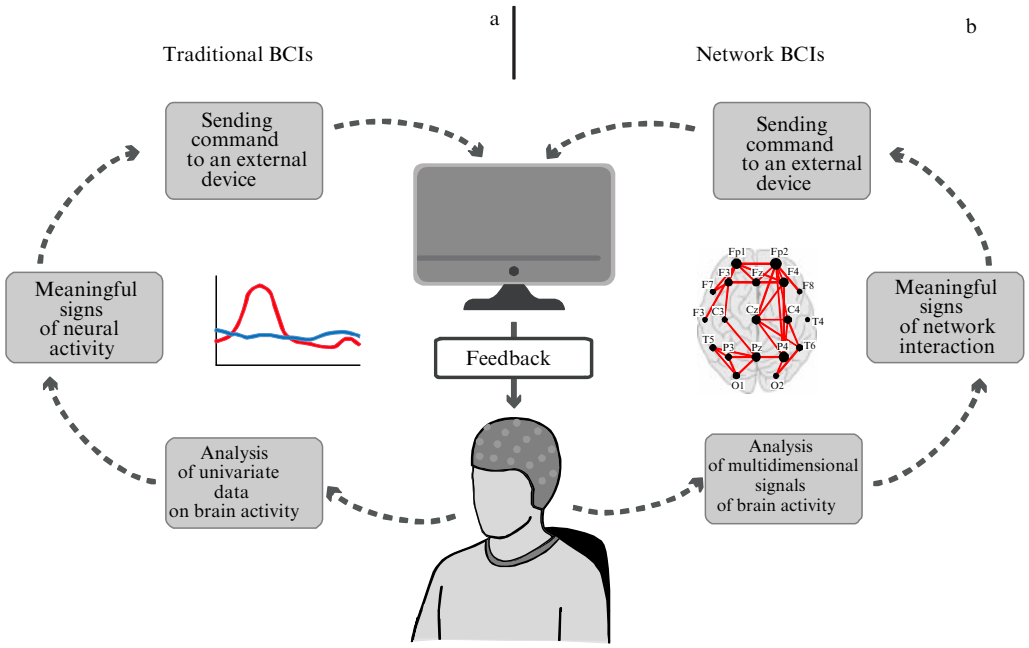

Figure 22. Schematic representation of the concepts of traditional BCIs (a) and network BCIs (b). Traditional BCIs identify meaningful signs based on signals from individual channels of multichannel data, whereas network BCIs analyze multidimensional signals of neural activity and highlight meaningful signs of network interaction in the brain.

band. Based on the analysis performed, the five most significant pairs of EEG signals were identified, the measure of synchronization between which significantly changes during imagination of a movement in comparison with that during background activity. The results suggest that the pairs of EEG sensors (Cz-Cp3) and (Fz, Cp4) are most informative for imaginary movements of the right and left hands, respectively. The results obtained suggest the possibility of using this algorithm in BCIs.

In a recent study [330], a new efficient algorithm for the classification of imaginary movements based on a two-level isolation of the network signs of brain activity was proposed. Initially, the minimum spanning tree method was applied to EEG signals to reconstruct the global network structure. At the second stage, local network structures were used to determine the network characteristics establishing a correspondence between the type of movement and the functional connectivity of cerebral cortex areas. The algorithm was tested using the open BCI Competition IV Dataset I database and demonstrated an accuracy of 89.50%, surpassing that of other classification methods applied to the same set of experimental data. This also suggests good prospects for using the 'network' approach as the algorithmic basis of motor BCIs.

The BCI technology also shows prospects for applications to problem solutions outside clinical and rehabilitation practice, e.g., to train cognitive functions in humans, including memory and learning ability. Earlier, attempts were made to create such BCIs based on the registration of local potentials [331–333], signals of activity from individual hippocampal neurons [334], evoked potentials, and evoked desynchronization [25, 240, 335].

Despite the fact that fundamental aspects of neurophysiology related to higher nervous activity are not yet fully understood, it is known that they are underlain by dynamic activation of distributed neuronal circuits [336]. Therefore, the optimal input parameters of BCIs for training cognitive functions could be the network characteristics of the reconstructed functional or effective connections in the brain. For example, the properties of functional connections reconstructed from multichannel EEG signals by the phase synchronization method were used to create BCIs for speech communication [337]. In this case, as in the classical virtual keyboard with a choice of characters using BCIs on the evoked P300 potential, the operator was presented with sets of characters that were sequentially highlighted on the screen [338–340]. The authors evaluated synchronization between the EEG channels when highlighting the letter of interest on the screen and in the absence of highlighting. A high degree of synchronization was shown between a certain number of EEG channels at time intervals corresponding to the processing of the letter. In addition, a high efficiency of the proposed network approach was shown in comparison with the traditional one based on the detection of the P300 potential when it was necessary to classify a large number of letters.

Mikulan et al. [341] have developed BCIs to classify sleep phases based on the assessment of phase synchronization in the upper γ-range (90–120 Hz) from intracranial EEG signals using a method for calculating the phase lag index (see Section 2.3.2, expression (13)) resistant to common source and bulk conductivity problems. It was shown that both the phase delay index itself and the degree of nodes are significantly higher in the state of waking than during sleep. In addition, the phase lag index in the upper γ-range (90–120 Hz) demonstrates more significant differences between sleep states than in the lower (30–60 Hz) and middle (60–90 Hz) γ-ranges, as well as in the θ-, α-, and β-ranges.

In a recent paper [342], a network interface was proposed to predict the efficiency of performance of a cognitive task in real time. The authors of [342] considered the reaction time of the subjects to a command exposed on a screen. They identified the intervals of fast and slow reactions and compared the average strength of connections in a functional network reconstructed using a phase synchronization measure. Significant differences in the average strength of connections in the network formed in a situation with the fast reaction compared with that for the slow reaction were observed in the pre-stimulus period. This finding made it possible to accurately predict the response rate in test subjects.

One more trend in the development of neurointerfaces is the construction of hybrid multimodal systems that use EEG and electromyography (EMG) signals to control assistive devices [343, 344]. Such devices find application in post-stroke neurorehabilitation with the use of robotic exoskeletons and prostheses with neural control [345]. The addition of electromyographic activity to motor-imaginary commands in the proper muscle groups increases the accuracy and reliability of their recognition. Moreover, a hybrid system actually involves the peripheral nervous system in the rehabilitation process of plastic rearrangements in the respective brain networks, which can significantly promote the restoration of sensorimotor coordination in the brain. Such work with multimodal signals opens up promising prospects for the use of network methods in the diagnostics of various states of the human nervous system.

It can be inferred that the network approach, together with the use of multimodal signals in the analysis of the active brain and the nervous system at large, not only provides a tool for investigating the fundamental aspects of the functioning of the distributed neural network in the brain but can also be successfully applied for the practical development of BCI technologies. The studies carried out thus far have demonstrated the applicability of the network approach to the creation of BCIs for motor function rehabilitation and the diagnostics and training of human cognitive functions.

5. Conclusion

This review was designed to analyze the current state and future prospects of an area of neuroscience developing in close cooperation with physics, mathematics, and information technologies, including machine learning and artificial intelligence methods for the study and reconstruction of cerebral functional networks. We tried to describe the motivation for such research, the setting of relevant tasks, and the most popular approaches to address them. Special attention was given to the correct reconstruction of functional connections based on the highly imperfect data provided by modern neuroimaging techniques and to the solution to arising problems. Equally great attention was given to the classification and comparison of modern physical and mathematical methods for reconstructing neuronal connections with special reference to the relationship among various methods. For some of the most widely used ones, additional calculations based on integrated experimental material were made to assess their relative value. We carried out an analysis of functional connections both at the sensory level (most

extensively used in scientific research and EEG/MEG experiments) and at the level of reconstruction of neuronal activity sources. Finally, we described the important limitations of both approaches that are likely to affect the correct interpretation of functional connections reconstructed from multichannel EEG/MEG data.

The review also considers examples of the application of functional networks and their analysis with the use of the mathematical apparatus of the graph theory to the interpretation of experimental data. We confined ourselves to three tasks of special importance from the fundamental and applied points of view: (1) processing a sequence of stimuli in the brain with subsequent decision-making based on the information obtained; (2) planning and controlling motor acts needed for the rehabilitation of patients presenting with cortical lesions, e.g., after a stroke; (3) analysis of functional connections in the thalamo-cortical network of the brain involved in the generation of an epileptic discharge. Finally, Section 4 discusses the possibility of real-time detection of the changes in the graph metric of the brain's functional network to create a 'network' brain–computer interface.

It is safe to infer that the development of increasingly more sophisticated methods for recording brain activity based on the progress in invasive [346, 347] and noninvasive [348, 349] technologies will further enhance the efficiency of approaches based on the reconstruction of functional and/or effective brain networks and thereby contribute to the understanding of brain functioning under normal and pathological conditions. The improvement of the quality of activity recording and the increased number of recorded channels coupled to the possibility for a more detailed observation of the brain regions of interest are expected to provide a deeper insight into the brain functioning mechanisms based on the continuous reorganization of cerebral networks and to promote the development of effective technologies for the early diagnostics and treatment of neurodegenerative diseases.

The reviewing of brain functional networks involved in processing sensory information and motor activity was supported by the Russian Science Foundation (grant 17-72-30003). The review of materials related to brain pathologies was carried out with the support of the Russian Foundation for Basic Research (grant 19-52-55001). The analysis of the use of the recurrent method for the diagnostics of functional connections was carried out in the framework of the Presidential Program for Support of Leading Scientific Schools (grant NSh-2594.2020.2).

References

1. Sporns O *Ann. New York Acad. Sci.* **1224** (1) 109 (2011)
2. Bullmore E, Sporns O *Nat. Rev. Neurosci.* **10** 186 (2009)
3. Kandel E R et al. *Principles of Neural Science* (Eds E R Kandel, J H Schwartz, T M Jessell) (New York: McGraw-Hill, 2000) Pt. 4
4. Buzsáki G *Rhythms of the Brain* (Oxford: Oxford Univ. Press, 2006)
5. Llinás R R *I of the Vortex*: *From Neurons to Self* (Cambridge, MA: MIT Press, 2001)
6. Borisyuk G N et al. *Phys. Usp.* **45** 1073 (2002); *Usp. Fiz. Nauk* **172** 1189 (2002)
7. Nekorkin V I *Phys. Usp.* **51** 295 (2008); *Usp. Fiz. Nauk* **178** 313 (2008)
8. Maslennikov O V, Nekorkin V I *Phys. Usp.* **60** 694 (2017); *Usp. Fiz. Nauk* **187** 745 (2017)
9. Abarbanel H D et al. *Phys. Usp.* **39** 337 (1996); *Usp. Fiz. Nauk* **166** 363 (1996)
10. Rabinovich M I et al. *Rev. Mod. Phys.* **78** 1213 (2006)
11. Izhikevich E M *Neural Comput.* **18** 245 (2006)
12. Chernavskii D S *Phys. Usp.* **43** 151 (2000); *Usp. Fiz. Nauk* **170** 157 (2000)
13. Bassett D S et al. *Proc. Natl. Acad. Sci. USA* **108** 7641 (2011)
14. Braun U et al. *Proc. Natl. Acad. Sci. USA* **112** 11678 (2015)
15. Finc K et al. *Nat. Commun.* **11** 2435 (2020)
16. Maksimenko V A et al. *Front. Behav. Neurosci.* **13** 220 (2019)
17. Zalesky A et al. *Proc. Natl. Acad. Sci. USA* **111** 10341 (2014)
18. Heeger D J, Ress D *Nat. Rev. Neurosci.* **3** 142 (2002)
19. Ferrari M, Quaresima V *NeuroImage* **63** 921 (2012)
20. Niedermeyer E, da Silva F L *Electroencephalography*: *Basic Principles, Clinical Applications, and Related Fields* (Philadelphia, PA: Lippincott Williams and Wilkins, 2005)
21. Baillet S *Nat. Neurosci.* **20** 327 (2017)
22. Hillebrand A et al. *Human Brain Mapping* **25** 199 (2005)
23. Smith S M et al. *NeuroImage* **54** 875 (2011)
24. Maksimenko V A et al. *Nonlinear Dyn.* **95** 1923 (2019)
25. Maksimenko V A et al. *Front. Neurosci.* **12** 949 (2018)
26. Betti V et al. *Neuron* **79** 782 (2013)
27. Maksimenko V A et al. *PloS One* **13** (9) e0197642 (2018)
28. Leonardi N, Van De Ville D *NeuroImage* **104** 430 (2015)
29. Friston K J et al. *NeuroImage* **56** 1202 (2011)
30. Seghier M L, Friston K J *NeuroImage* **68** 181 (2013)
31. Boccaletti S et al. *Phys. Rep.* **424** 175 (2006)
32. Zou Y et al. *Phys. Rep.* **787** 1 (2019)
33. Rubinov M, Sporns O *NeuroImage* **52** 1059 (2010)
34. Telesford Q K et al. *Brain Connectivity* **1** 295 (2011)
35. Sporns O *Curr. Opin. Neurobiol.* **23** 162 (2013)
36. Vecchio F, Miraglia F, Rossini P M *Clin. Neurophysiol. Pract.* **2** 206 (2017)
37. Vergotte G et al. *Biomed. Opt. Express* **8** 5326 (2017)
38. Hilger K et al. *Sci. Rep.* **7** 16088 (2017)
39. Fleischer V et al. *Neuroscience* **403** 35 (2019)
40. Curley J P, Ochsner K N *Nat. Hum. Behav.* **1** 0104 (2017)
41. Ekstrom A D, Huffman D J, Starrett M *J. Neurophysiol.* **118** 3328 (2017)
42. Richmond S et al. *Neurosci. Biobehav. Rev.* **71** 215 (2016)
43. Sala-Llonch R, Bartrés-Faz D, Junqué C *Front. Psychol.* **6** 663 (2015)
44. Sporns O *Networks of the Brain* (Cambridge, MA: MIT Press, 2011)
45. Calhoun V D, Eichele T, Pearlson G *Front. Human Neurosci.* **3** 17 (2009)
46. Smith S M et al. *Proc. Natl. Acad. Sci. USA* **106** 13040 (2009)
47. Cole M W et al. *Neuron* **83** 238 (2014)
48. Hearne L J, Mattingley J B, Cocchi L *Sci. Rep.* **6** 32328 (2016)
49. Li F et al. *IEEE Trans. Neural Syst. Rehabilit. Eng.* **27** 594 (2019)
50. Li F et al. *Brain Topography* **32** 304 (2019)
51. Friston K J *Brain Connect* **1** 13 (2011)
52. Verkhratsky A, Butt S *Glial Neurobiology*: *a Textbook* (Hoboken, NJ: John Wiley and Sons, 2007)
53. Dityatev A, Wehrle-Haller B, Pitkänen A (Eds) *Brain Extracellular Matrix in Health and Disease* (Progress in Brain Research, Vol. 214) (Amsterdam: Elsevier, 2014)
54. van Ooyen A, Ribchester R R, in *Modeling Neural Development* (Ed. A van Ooyen) (Cambridge, MA: Bradford Book, 2003) p. 183
55. Borisyuk R et al. *PLoS One* **9** (2) e89461 (2014)
56. Wig G S, Schlaggar B L, Petersen S E *Ann. New York Acad. Sci.* **1224** (1) 126 (2011)
57. Bastos A M, Schoffelen J M *Front. Syst. Neurosci.* **9** 175 (2016)
58. Hramov A E et al. *Sensors* **20** 2362 (2020)
59. Sakkalis V *Comput. Biol. Med.* **41** 1110 (2011)
60. Hramov A E et al. *Wavelets in Neuroscience* (Berlin: Springer, 2015)
61. Li K et al. *Comput. Med. Imag. Graph.* **33** (2) 131 (2009)
62. BlinowskaK J *Med. Biol. Eng. Comput.* **49** 521 (2011)
63. Maris E, Oostenveld R *J. Neurosci. Meth.* **164** 177 (2007)
64. Nunez P L, Srinivasan R *Electric Fields of the Brain*: *the Neurophysics of EEG* (Oxford: Oxford Univ. Press, 2006)
65. Schoffelen J-M, Gross J *Human Brain Mapping* **30** 1857 (2009)
66. Hamedi M, Salleh S H, Noor A M *Neural Comput.* **28** 999 (2016)
67. Vinck M et al. *NeuroImage* **55** 1548 (2011)
68. Nolte G et al. *Clin. Neurophysiol.* **115** 2292 (2004)

69. Nolte G et al., in *Proc. of Workshop on Causality: Objectives and Assessment at NIPS 2008* (Proc. of Machine Learning Research, Vol. 6, Eds I Guyon et al.) (Long Beach, CA: MLResearchPress, 2010) p. 267
70. Hyvärinen A et al. *J. Machine Learning Res.* **11** 1709 (2010)
71. Faes L, Nollo G *Biol. Cybernet.* **103** 387 (2010)
72. Mamashli F et al. *Sci. Rep.* **9** 7942 (2019)
73. Hassan M, Wendling F *IEEE Signal Process. Mag.* **35** 81 (2018)
74. David O, Friston K J *NeuroImage* **20** 1743 (2003)
75. Baillet S, Mosher J C, Leahy R M *IEEE Signal Process. Mag.* **18** (6) 14 (2001)
76. Nolte G, Curio G *IEEE Trans. Biomed. Eng.* **47** 1347 (2000)
77. Mosher J C, Leahy R M, Lewis P S *IEEE Trans. Biomed. Eng.* **46** 245 (1999)
78. Zhang Z *Phys. Med. Biol.* **40** 335 (1995)
79. Shattuck D W et al. *NeuroImage* **13** 856 (2001)
80. Ermer J J et al. *Phys. Med. Biol.* **46** 1265 (2001)
81. Nolte G *Phys. Med. Biol.* **48** 3637 (2003)
82. Grech R et al. *J. Neuroeng. Rehabilit.* **5** (1) 25 (2008)
83. Greenblatt R E, Pflieger M E, Ossadtchi A E *J. Neurosci. Meth.* **207** 1 (2012)
84. Pascual-Marqui R D *Int. J. Bioelectromag.* **1** (1) 75 (1999)
85. Groβ J et al. *Proc. Natl. Acad. Sci. USA* **98** 694 (2001)
86. Kurkin S et al., in *2020 4th Intern. Conf. on Computational Intelligence and Networks, CINE* (Piscataway, NJ: IEEE, 2020) p. 1
87. Oostenveld R et al. *Comput. Intelligence Neurosci.* **2011** 156869 (2011)
88. Garrido M I et al. *NeuroImage* **36** 571 (2007)
89. Kiebel S J et al. *Cognitive Neurodyn.* **2** (2) 121 (2008)
90. Chen C, Kiebel S J, Friston K J *NeuroImage* **41** 1293 (2008)
91. Moran R J et al. *NeuroImage* **37** 706 (2007)
92. Babiloni F et al. *NeuroImage* **24** 118 (2005)
93. Astolfi L et al. *Mag. Reson. Imaging* **22** 1457 (2004)
94. Astolfi L et al. *Clin. Neurophysiol.* **116** 920 (2005)
95. Lin F H et al. *NeuroImage* **23** 582 (2004)
96. Groß J et al. *Proc. Natl. Acad. Sci. USA* **99** 2299 (2002)
97. Timmermann L et al. *Brain* **126** 199 (2002)
98. Pollok B et al. *J. Physiol.* **554** 871 (2004)
99. Schnitzler A, Gross J *Nat. Rev. Neurosci.* **6** 285 (2005)
100. Jerbi K et al. *Proc. Natl. Acad. Sci. USA* **104** 7676 (2007)
101. Schoffelen J M, Oostenveld R, Fries P *NeuroImage* **41** 437 (2008)
102. David O et al. *IEEE Trans. Biomed. Eng.* **49** 975 (2002)
103. Kujala J et al. *Cerebral Cortex* **17** 1476 (2007)
104. Kujala J, Gross J, Salmelin R *NeuroImage* **39** 1706 (2008)
105. Dossevi A et al. *IEEE Trans. Biomed. Eng.* **55** 2074 (2008)
106. Gómez-Herrero G et al. *NeuroImage* **43** 497 (2008)
107. Marzetti L, Del Gratta C, Nolte G *NeuroImage* **42** 87 (2008)
108. Wittevrongel B, Van Hulle M M *Front. Neurosci.* **11** 630 (2017)
109. Coito A et al. *IEEE Trans. Biomed. Eng.* **63** 2619 (2016)
110. Muthuraman M et al. *Sci. Rep.* **9** 20028 (2019)
111. Lelic D et al. *NeuroImage* **60** 37 (2012)
112. Gao L et al. *Sci. Rep.* **5** 10399 (2015)
113. Mahjoory K et al. *NeuroImage* **152** 590 (2017)
114. Groβ J et al. *NeuroImage* **19** 1329 (2003)
115. Barnes G R et al. *Human Brain Mapping* **23** 120 (2004)
116. Glasser M F et al. *Nature* **536** 171 (2016)
117. Frolov N, et al. *Chaos* **29** 091101 (2019)
118. Hoechstetter K et al. *Brain Topography* **16** 233 (2004)
119. Pollok B et al. *Cognitive Brain Res.* **25** 300 (2005)
120. Pijn J et al. *Adv. Epileptology* **17** 272 (1989)
121. da Silva F L, Pijn J P, Boeijinga P *Brain Topography* **2** 9 (1989)
122. Pecora L M, Carroll T L *Phys. Rev. Lett.* **64** 821 (1990)
123. Pikovsky A, Rosenblum M, Kurths J *Synchronization: a Universal Concept in Nonlinear Sciences* (The Cambridge Nonlinear Science Ser., Vol. 12) (Cambridge: Cambridge Univ. Press, 2003)
124. Rosenblum M G, Pikovsky A S, Kurths J *Phys. Rev. Lett.* **76** 1804 (1996)
125. Varela F et al. *Nat. Rev. Neurosci.* **2** 229 (2001)
126. Fell J, Axmacher N *Nat. Rev. Neurosci.* **12** 105 (2011)
127. Hramov A E, Koronovskii A A, Levin Y I *J. Exp. Theor. Phys.* **100** 784 (2005); *Zh. Eksp. Teor. Fiz.* **127** 886 (2005)
128. Lachaux J P et al. *Human Brain Mapping* **8** 194 (1999)
129. Rosenblum M, Kurths J, in *Nonlinear Analysis of Physiological Data* (Eds H Kantz, J Kurths, G Mayer-Kress) (Berlin: Springer, 1998) p. 91
130. Halliday D et al. *Prog. Biophys. Mol. Biol.* **64** 237 (1995)
131. Nolte G et al. *Phys. Rev. Lett.* **100** 234101 (2008)
132. Stam C J, Nolte G, Daffertshofer A *Human Brain Mapping* **28** 1178 (2007)
133. Van Milligen B P et al. *Phys. Plasmas* **2** 3017 (1995)
134. Koronovskii A A, Hramov A E *Plasma Phys. Rep.* **28** 666 (2002); *Fiz. Plazmy* **28** 722 (2002)
135. Pisarchik A N et al. *Sci. Rep.* **9** 18325 (2019)
136. Hramov A E et al. *Chaos* **29** 093110 (2019)
137. Makarov V V et al. *Phys. Rev. E* **98** 062413 (2018)
138. Cover T M, Thomas J A *Elements of Information Theory* (New York: John Wiley and Sons, 2012)
139. Ioannides A et al. *Human Brain Mapping* **11** 77 (2000)
140. Liu L, Ioannides A A *NeuroImage* **31** 1726 (2006)
141. Jeong J, Gore J C, Peterson B S *Clin. Neurophysiol.* **112** 827 (2001)
142. Ioannides A, Bolton J, Clarke C *Inverse Probl.* **6** 523 (1990)
143. Rulkov N F et al. *Phys. Rev. E* **51** 980 (1995)
144. Hramov A, Koronovskii A, Moskalenko O *Europhys. Lett.* **72** 901 (2005)
145. Koronovskii A A, Moskalenko O I, Hramov A E *Phys. Rev. E* **84** 037201 (2011)
146. Pecora L M, Carroll T L *Chaos* **25** 097611 (2015)
147. Moskalenko O I et al. *Phys. Rev. E* **86** 036216 (2012)
148. Takens F, in *Dynamical Systems and Turbulence, Warwick 1980: Proc. of a Symp, Univ. of Warwick 1979-80* (Lecture Notes in Mathematics, Vol. 898, Eds D A Rand, L-S Young) (Berlin: Springer-Verlag, 1981) p. 366
149. Kennel M B, Brown R, Abarbanel H D I *Phys. Rev. A* **45** 3403 (1992)
150. Roulston M S *Physica D* **125** 285 (1999)
151. Marwan N et al. *Phys. Rep.* **438** 237 (2007)
152. Romano M C et al. *Europhys. Lett.* **71** 466 (2005)
153. Goswami B et al. *Eur. Phys. J. ST* **222** 861 (2013)
154. Ouyang G et al. *IEEE J. Bomed. Health Inform.* **18** 257 (2013)
155. Builes-Jaramillo A et al. *Climate Dynamics* **50** 2951 (2018)
156. Goodfellow I, Bengio Y, Courville A *Deep Learning* (Cambridge, MA: The MIT Press, 2016) p. 168
157. Hornik K et al. *Neural Networks* **2** 359 (1989)
158. Cybenko G *Math. Control Signal Systems* **2** 303 (1989)
159. Friston J, Harrison L, Penny, W *NeuroImage* **19** 1273 (2003)
160. Morris C, Lecar H *Biophys. J.* **35** 193 (1981)
161. Friston K, in *Statistical Parametric Mapping: the Analysis of Funtional Brain Images* (Eds K Friston et al.) (Amsterdam: Elsevier. Academic Press, 2007) p. 606
162. Rigoux L et al. *NeuroImage* **84** 971 (2014)
163. Friston K J et al. *NeuroImage* **128** 413 (2016)
164. Granger C W *Econometrica* **37** 424 (1969)
165. Akaike H, in *Selected Papers of Hirotugu Akaike* (Berlin: Springer, 1998) p. 199
166. Schwarz G et al. *Ann. Statist.* **6** 461 (1978)
167. Hiemstra C, Jones J D *J. Finance* **49** 1639 (1994)
168. Marinazzo D, Pellicoro M, Stramaglia S *Phys. Rev. Lett.* **100** 144103 (2008)
169. Sysoeva M V et al. *J. Neurosci. Meth.* **226** 33 (2014)
170. Geweke J *J. Am. Stat. Association* **77** 304 (1982)
171. Kaminski M J, Blinowska K J *Biol. Cybern.* **65** 203 (1991)
172. Sameshima K, Baccalá L A *J. Neurosci. Meth.* **94** 93 (1999)
173. Schlögl A, Supp G *Prog. Brain Res.* **159** 135 (2006)
174. Kamiński M, Liang H *Critical Rev. Biomed. Eng.* **33** 347 (2005)
175. Baccalá L A, Sameshima K *Biol. Cybern.* **84** 463 (2001)
176. Supp G G et al. *PloS One* **2** (8) e684 (2007)
177. Gow Jr D W et al. *NeuroImage* **43** 614 (2008)
178. Astolfi L et al. *IEEE Trans. Biomed. Eng.* **55** 902 (2008)
179. Davison E N et al. *PLoS Comput. Biol.* **11** e1004029 (2015)
180. Shine J M, Poldrack R A *NeuroImage* **180** 396 (2018)
181. Parks E L, Madden D J *Brain Connectivity* **3** 317 (2013)
182. Smith S *Nat. Neurosci.* **19** (1) 7 (2016)
183. Van Den Heuvel M P, Pol H E H *Europ. Neuropsychopharmacology* **20** 519 (2010)
184. Xu J, Potenza M N, Calhoun V D *Front. Neurosci.* **7** 154 (2013)

185. Li J et al. *Front. Human Neurosci.* **10** 304 (2016)
186. Finc K et al. *Human Brain Mapping* **38** 3659 (2017)
187. Papo D *Philos. Trans. R. Soc. Lond. B* **369** 20130520 (2014)
188. Wang L et al. *Ann. Appl. Stat.* **13** 85 (2019)
189. Bollobás B *Modern Graph Theory* (Graduate Texts in Mathematics, Vol. 184) (Berlin: Springer, 2013)
190. Sporns O *Front. Comput. Neurosci.* **5** 5 (2011)
191. Rubinov M, Sporns O *NeuroImage* **56** 2068 (2011)
192. Watts D J, Strogatz S H *Nature* **393** 440 (1998)
193. Kaiser M, Hilgetag C C *PLoS Comput. Biol.* **2** (7) e95 (2006)
194. He Y et al. *PloS One* **4** (4) (2009)
195. Meunier D, Lambiotte R, Bullmore E T *Front. Neurosci.* **4** 200 (2010)
196. Bullmore E, Sporns O *Nat. Rev. Neurosci.* **13** 336 (2012)
197. Wang Z et al. *Neuroscience* **21** 290 (2015)
198. Rudie J D et al. *NeuroImage*: *Clinical* **2** 79 (2013)
199. Van den Heuvel M P, Sporns O *J. Neurosci.* **33** 14489 (2013)
200. Sporns O, Honey C J, Kötter R *PloS One* **2** (10) e1049 (2007)
201. Van Den Heuvel M P, Sporns O *J. Neurosci.* **31** 15775 (2011)
202. Van den Heuvel M P, Sporns O *Trends Cognitive Sci.* **17** 683 (2013)
203. Collin G et al. *Cerebral Cortex* **24** 2258 (2014)
204. Collin G et al. *Schizophrenia Bull.* **40** 438 (2014)
205. Zamora-López G, Zhou C, Kurths J *Front. Neuroinform.* **4** 1 (2010)
206. Van den Heuvel M P et al. *Proc. Natl. Acad. Sci. USA* **109** 11372 (2012)
207. Schirmer M D et al. *Front. Neurology* **10** 956 (2019)
208. Gleichgerrcht E et al. *Restorative Neurology Neurosci.* **34** (1) 19 (2016)
209. Smit D J et al. *Human Brain Mapping* **29** 1368 (2008)
210. Eguiluz V M et al. *Phys. Rev. Lett.* **94** 018102 (2005)
211. Hagmann P et al. *PloS One* **2** (7) e597 (2007)
212. Van den Heuvel M P et al. *NeuroImage* **43** 528 (2008)
213. Hagmann P et al. *PLoS Biology* **6** (7) e159 (2008)
214. Mears D, Pollard H B *J. Neurosci. Res.* **94** 590 (2016)
215. Bassett D S et al. *Proc. Natl. Acad. Sci. USA* **106** 11747 (2009)
216. Van Den Heuvel M P et al. *J. Neurosci.* **29** 7619 (2009)
217. Zhou S, Mondragón R J *IEEE Commun. Lett.* **8** 180 (2004)
218. McAuley J J, da Fontoura Costa L, Caetano T S *Appl. Phys. Lett.* **91** 084103 (2007)
219. Colizza V et al. *Nat. Phys.* **2** 110 (2006)
220. Senden M et al. *NeuroImage* **96** 174 (2014)
221. Grayson D S et al. *PloS One* **9** (2) e88297 (2014)
222. Liang X et al. *Cerebral Cortex* **28** 924 (2018)
223. Girvan M, Newman M E *Proc. Natl. Acad. Sci. USA* **99** 7821 (2002)
224. Radicchi F et al. *Proc. Natl. Acad. Sci. USA* **101** 2658 (2004)
225. Fortunato S, Latora V, Marchiori M *Phys. Rev. E* **70** 056104 (2004)
226. Du Y, Wang J, Li Q *IEEE Access* **5** 17478 (2017)
227. Baniqued P L et al. *Front. Aging Neurosci.* **9** 426 (2018)
228. Muthuraman M et al. *Front. Neurosci.* **10** 14 (2016)
229. Telesford Q K et al. *NeuroImage* **142** 198 (2016)
230. Collin G et al. *Schizophrenia Res.* **173** 166 (2016)
231. Van den Heuvel M P et al. *J. Neurosci.* **30** 15915 (2010)
232. Giedd J N et al. *Neuropsychol. Rev.* **20** 349 (2010)
233. Collin G, van den Heuvel M P, in *The Neurobiology of Schizophrenia* (Eds T Abel, T Nickl-Jockschat) (Amsterdam: Elsevier, 2016) p. 313
234. Alexander-Bloch A F et al. *Bullmore Front. Syst. Neurosci.* **4** 147 (2010)
235. Bassett D S et al. *Proc. Natl. Acad. Sci. USA* **103** 19518 (2006)
236. Liao X H et al. *NeuroImage* **83** 969 (2013)
237. Sasai S et al. *Front. Human Neurosci.* **8** 1022 (2014)
238. Thompson W H, Fransson P *NeuroImage* **121** 227 (2015)
239. De Domenico M, Sasai S, Arenas A *Front. Neurosci.* **10** 326 (2016)
240. Maksimenko V A et al. *PloS One* **12** (12) e0188700 (2017)
241. Assaf Y, Pasternak O *J. Mol. Neurosci.* **34** 51 (2008)
242. Muldoon S F, Bassett D S *Philos. Sci.* **83** 710 (2016)
243. De Domenico M *Giga Sci.* **6** (5) gix004 (2017)
244. Vaiana M, Muldoon S F *J. Nonlin. Sci.* 1–23 (2018)
245. De Domenico M et al. *Phys. Rev. X* **3** 041022 (2013)
246. Boccaletti S et al. *Phys. Rep.* **544** 1 (2014)
247. Battiston F et al. *Chaos* **27** 047404 (2017)
248. Buldú J M, Porter M A *Network Neurosci.* **2** 418 (2018)
249. Yu M et al. *Brain* **140** 1466 (2017)
250. Brookes M J et al. *NeuroImage* **132** 425 (2016)
251. Tewarie P et al. *NeuroImage* **142** 324 (2016)
252. Kanawati R *IEEE Intell. Inform. Bull.* **16** (1) 24 (2015)
253. Buschman T J, Miller E K *Science* **315** 1860 (2007)
254. Gazzaley A, Nobre A C *Trends Cognitive Sci.* **16** (2) 129 (2012)
255. Schafer R J, Moore T *Science* **332** 1568 (2011)
256. Markov N T et al. *J. Comparative Neurology* **522** 225 (2014)
257. Muckli L et al. *Current Biol.* **25** 2690 (2015)
258. Michalareas G et al. *Neuron* **89** 384 (2016)
259. Maksimenko V A et al. *Phys. Rev. E* **97** 052405 (2018)
260. Frolov N S et al. *Eur. Phys. J. ST* **228** 2381 (2019)
261. Laufs H et al. *NeuroImage* **31** 1408 (2006)
262. Berger B et al. *Nat. Commun.* **10** 4242 (2019)
263. Pikovsky A S, Kurths J *Phys. Rev. Lett.* **78** 775 (1997)
264. Neiman A, Saparin P I, Stone L *Phys. Rev. E* **56** 270 (1997)
265. Palenzuela C et al. *Europhys. Lett.* **56** 347 (2001)
266. Andreev A V et al. *Chaos Solitons Fractals* **106** 80 (2018)
267. Pisarchik A, Jaimes-Reátegui R *Phys. Rev. E* **92** 050901 (2015)
268. Yilmaz E et al. *Sci. Rep.* **6** 30914 (2016)
269. Paszek P et al. *Proc. Natl. Acad. Sci. USA* **107** 11644 (2010)
270. Kellogg R A, Tay S *Cell* **160** 381 (2015)
271. Ermentrout G B, Galán R F, Urban N N *Trends Neurosci.* **31** 428 (2008)
272. Tolhurst D, Movshon J A, Thompson I *Exp. Brain Res.* **41** 414 (1981)
273. Runnova A E et al. *Chaos Solitons Fractals* **93** 201 (2016)
274. Hramov A E et al. *Chaos* **28** 033607 (2018)
275. Mostert P, Kok P, De Lange F P *Sci. Rep.* **5** 18253 (2015)
276. Ramos A M et al. *Phys. Rev. E* **95** 052206 (2017)
277. Maksimenko V A et al. *Inform.-Upravlyayushchie Sist.* (1) 73 (2020)
278. Leisman G, Braun-Benjamin O, Melillo R *Front. Syst. Neurosci.* **8** 16 (2014)
279. Leisman G, Moustafa A A, Shafir T *Front. Public Health* **4** 94 (2016)
280. Vallortigara G, Rogers L J, Bisazza A *Brain Res. Rev.* **30** (2) 164 (1999)
281. Carruthers P *Proc. Natl. Acad. Sci. USA* **110** (Suppl. 2) 10371 (2013)
282. Koziol L F et al. *Cerebellum* **13** (1) 151 (2014)
283. Dijkstra K, Kaschak M P, Zwaan R A *Cognition* **102** 139 (2007)
284. Grefkes C et al. *Ann. Neurology* **63** 236 (2008)
285. Gao Q, Duan X, Chen H *NeuroImage* **54** 1280 (2011)
286. Stephan K E et al. *NeuroImage* **49** 3099 (2010)
287. Chholak P et al. *Sci. Rep.* **9** (1) 1 (2019)
288. Neuper C et al. *Cognitive Brain Res.* **25** 668 (2005)
289. Bufalari I et al. *Cerebral Cortex* **17** 553 (2007)
290. Hanakawa T et al. *J. Neurophysiology* **89** (2) 989 (2003)
291. Inman C S et al. *NeuroImage* **59** 227 (2012)
292. Silasi G, Murphy T H *Neuron* **83** 1354 (2014)
293. Mintzopoulos D et al. *NeuroImage* **47** T90 (2009)
294. Jiang L, Xu H, Yu C *Neural Plasticity* **2013** 924192 (2013)
295. Bajaj S et al. *Front. Systems Neurosci.* **8** 13 (2014)
296. Bajaj S et al. *Front. Human Neurosci.* **9** 173 (2015)
297. Grefkes C, Fink G R *Lancet Neurology* **13** (2) 206 (2014)
298. Bajaj S et al. *NeuroImage Clinical* **8** 572 (2015)
299. Fugl-Meyer A R et al. *Scandinavian J. Rehabilit. Med.* **7** (1) 13 (1975)
300. Coenen A, Van Luijtelaar E *Behavior Genetics* **33** 635 (2003)
301. Maksimenko V A et al. *Phys. Rev. E* **96** 012316 (2017)
302. Van Luijtelaar G et al. *J. Neurosci. Meth.* **260** 144 (2016)
303. Sarkisova K, van Luijtelaar G *Prog. Neuro-Psychopharmacol. Biol. Psychiatry* **35** 854 (2011)
304. Sitnikova E et al. *J. Neurosci. Meth.* **180** 304 (2009)
305. Sitnikova E et al. *Brain Res.* **1543** 290 (2014)
306. Pavlov A N et al. *Phys. Usp.* **55** 845 (2012); *Usp. Fiz. Nauk* **182** 905 (2012)
307. Maksimenko V A et al. *Sci. Rep.* **7** 2487 (2017)
308. Sysoeva M et al. *Neuroscience* **314** 75 (2016)
309. Lüttjohann A, van Luijtelaar G *Neurobiol. Disease* **47** 49 (2012)
310. Lüttjohann A, Schoffelen J M, Van Luijtelaar G *Exp. Neurology* **239** 235 (2013)
311. Vinck M et al. *NeuroImage* **51** 112 (2010)
312. Van Luijtelaar G et al. *Clin. Neurophysiol.* **122** 687 (2011)
313. Chaudhary U, Birbaumer N, Ramos-Murguialday A *Nat. Rev. Neurology* **12** 513 (2016)
314. Hramov A E et al. *Phys. Rev. E* **75** 056207 (2007)

315. McFarland D J, Wolpaw J R *J. Neural Eng.* **5** 155 (2008)
316. Yuan H, He B *IEEE Trans. Biomed. Eng.* **61** 1425 (2014)
317. Lebedev M A, Nicolelis M A *Physiol. Rev.* **97** 767 (2017)
318. Frolov A A et al. *Front. Neurosci.* **11** 400 (2017)
319. Babiloni C et al. *NeuroImage* **10** 658 (1999)
320. Pfurtscheller G et al. *NeuroImage* **31** 153 (2006)
321. Pitsik E et al. *Chaos* **30** 023111 (2020)
322. Benabid A L et al. *Lancet Neurol.* **18** 1112 (2019)
323. Lotte F et al. *J. Neural Eng.* **4** R1 (2007)
324. McFarland D, Wolpaw J *Curr. Opin. Biomed. Eng.* **4** 194 (2017)
325. Kam T E, Suk H I, Lee S W *Neurocomputing* **108** 58 (2013)
326. Asensio-Cubero J, Gan J, Palaniappan R *J. Neural Eng.* **10** 046014 (2013)
327. Daly I, Nasuto S J, Warwick K *Pattern Recognition* **45** 2123 (2012)
328. Billinger M, Brunner C, Müller-Putz G R *J. Neural Eng.* **10** 046006 (2013)
329. Gonuguntla V, Wang Y, Veluvolu K C, in *2013 35th Annual International Conf. of the IEEE Engineering in Medicine and Biology Society, EMBC* (Piscataway, NJ: IEEE, 2013) p. 2784
330. Luo Z, Lu X, Xi X *Electronics* **9** 203 (2020)
331. Sederberg P B et al. *Cerebral Cortex* **17** 1190 (2007)
332. Fell J et al. *J. Neurosci.* **31** 5392 (2011)
333. Hanslmayr S, Staudigl T *NeuroImage* **85** 648 (2014)
334. Rutishauser U et al. *Nature* **464** 903 (2010)
335. Nicolae I E, Acqualagna L, Blankertz B *Front. Neurosci.* **11** 548 (2017)
336. FitzGerald T H, Friston K J, Dolan R J *J. Neurosci.* **32** 16417 (2012)
337. Kabbara A et al. *PLoS One* **11** (1) e0146282 (2016)
338. Donchin E, Spencer K M, Wijesinghe R *IEEE Trans. Rehabilitat. Eng.* **8** 174 (2000)
339. Panicker R C, Puthusserypady S, Sun Y *IEEE Trans. Biomed. Eng.* **58** 1781 (2011)
340. Fazel-Rezai R et al. *Front. Neuroeng.* **5** 14 (2012)
341. Mikulan E et al. *NeuroImage* **169** 265 (2018)
342. Buch V P et al. *Front. Neurosci.* **12** 790 (2018)
343. Kirchner E A, Tabie M, Seeland A *PloS One* **9** (1) e85060 (2014)
344. Grimm F et al. *Front. Neurosci.* **10** 367 (2016)
345. Gordleeva S Yu et al. *IEEE Access* **8** 84070 (2020)
346. Musk E et al. *J. Med. Internet Res.* **21** e16194 (2019)
347. Pisarchik A N, Maksimenko V A, Hramov A E *J. Med. Internet Res.* **21** e16356 (2019)
348. Ford J P, Sudre G P "Methods and magnetic imaging devices to inventory human brain cortical function", US Patent App. 16/151, 105 (2019)
349. Wu T et al. *Bull. Am. Phys. Soc.* **65** (4) S07.00008 (2020)